CHAPTER 3: RESULTS

3.1 Gross Morphology of Frog Spinal Cord

The spinal cord of the frog was characterised by an elongated, tubular bundle of nerve tissues that was housed within the canal of a vertebral column (Figure 3.1, Figure 3.2). It was observed that the length of the spinal cord was shorter than the column itself. This delicate tissue was continuous from the most posterior of the hindbrain i.e. medulla oblongata, and extended caudally to a tapering, slender cone known as the conus medullaris. Coming from the conus medullaris was filum terminale, a threadlike string of connective tissue. Two distinct longitudinal grooves were observed on each surface side of the structure, separating the left and right symmetrical halves throughout the length of the cord. As a deep groove along the median plane of the ventral side, the anterior median fissure was relatively more prominent in comparison to the posterior median sulcus, which was barely noticeable from the dorsal view (Figure 3.3, Figure 3.4).

The spinal cord was subdivided into segments with a pair of spinal nerves exiting from each intervertebral foramina that divides to form dorsal and ventral roots. Four distinct segments of the spinal cord, from rostral to caudal, namely cervical, thoracic, lumbar and sacral were differentiated based on the circumferential thickness at each particular level that could be easily visualised with the naked eye. The cervical segment was located below the fourth ventricle of the hindbrain (Figure 3.4). Unlike the ventricles in other parts of the brain, the fourth ventricle was not enclosed by the nervous tissues. The thoracic region was marked by a slight narrowing of the cord from the caudal part of cervical region. Shortly below the thoracic region, the cord exhibited subtle enlargement at the lumbar segment before alternately reduced in circumferential cord size at the sacral region. Localised enlargements at the cervical and lumbar spinal regions were reflected by the size of their transverse sections as they were relatively

larger than those of thoracic and sacral segments (Figure 3.3, Figure 3.4, Figure 3.5). This statement is further verified in the subchapter 3.2.1 with digital measurements (transverse and vertical diameters of each representative transverse section of the spinal segment) being taken using the mentioned software in photomicrographs analysis.

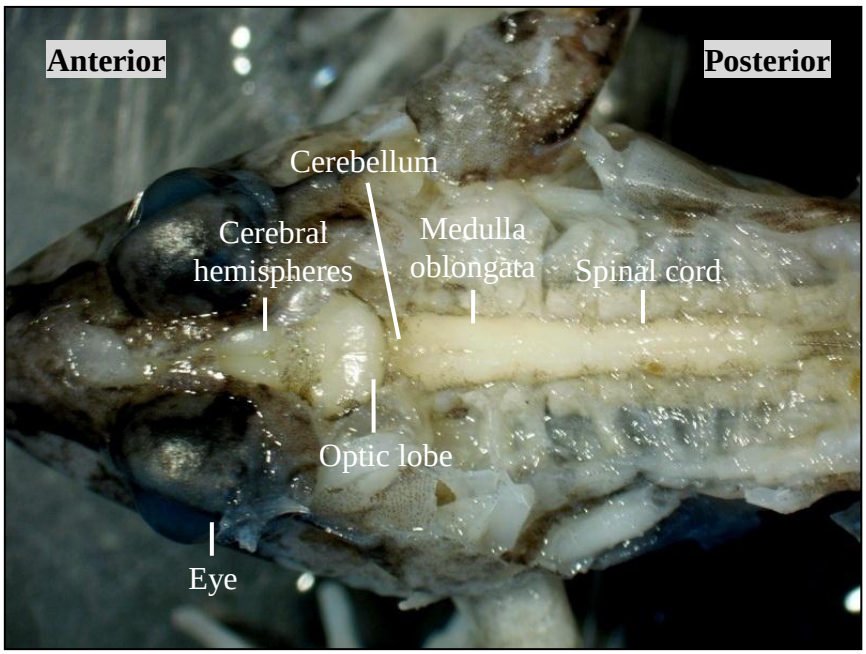

Figure 3.1: Dorsal view of the central nervous system of *Fejervarya limnocharis*.

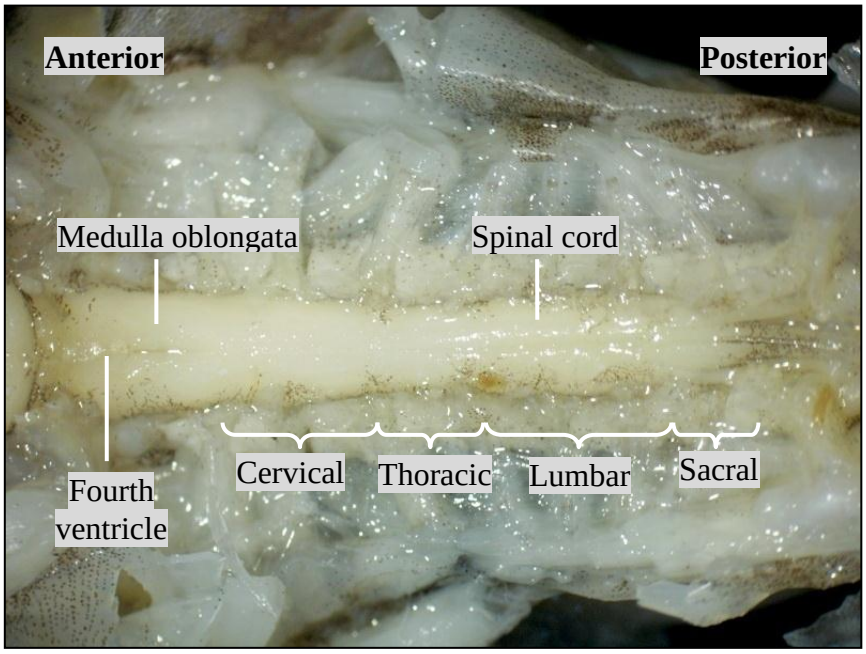

Figure 3.2: Dorsal view of the spinal cord of *Fejervarya limnocharis*.

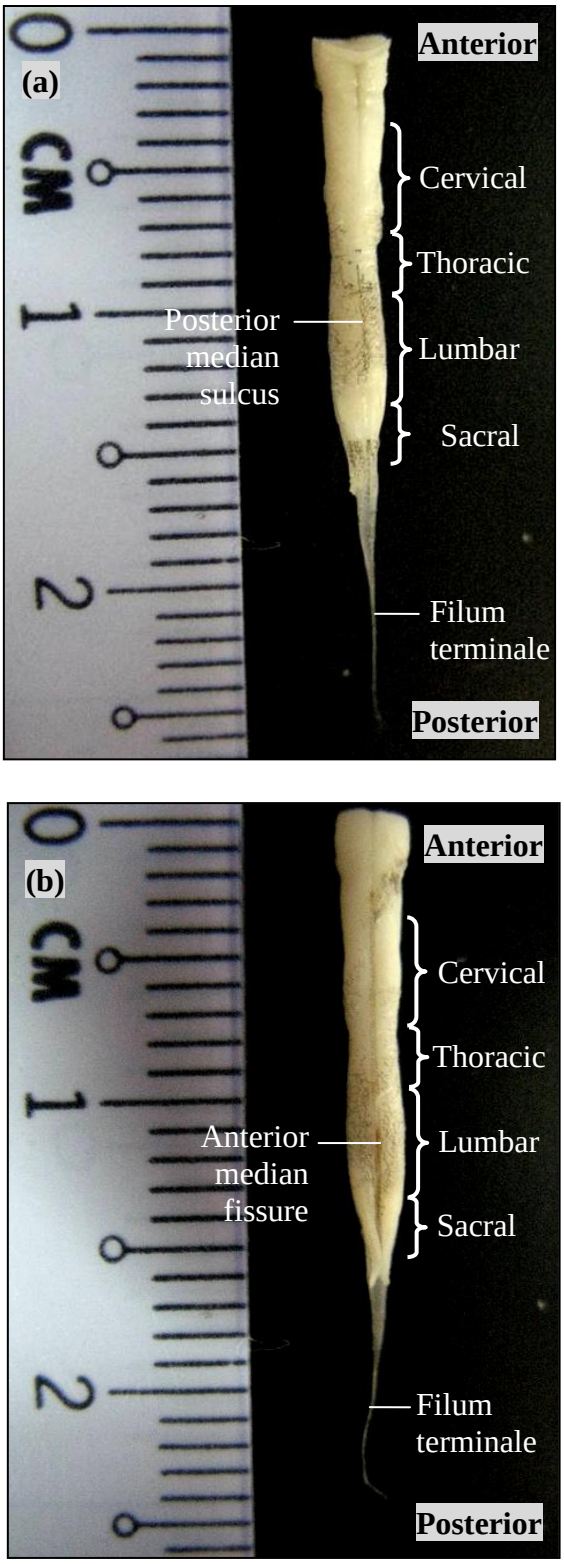

Figure 3.3: Frog spinal cord; (a) dorsal view, (b) ventral view.

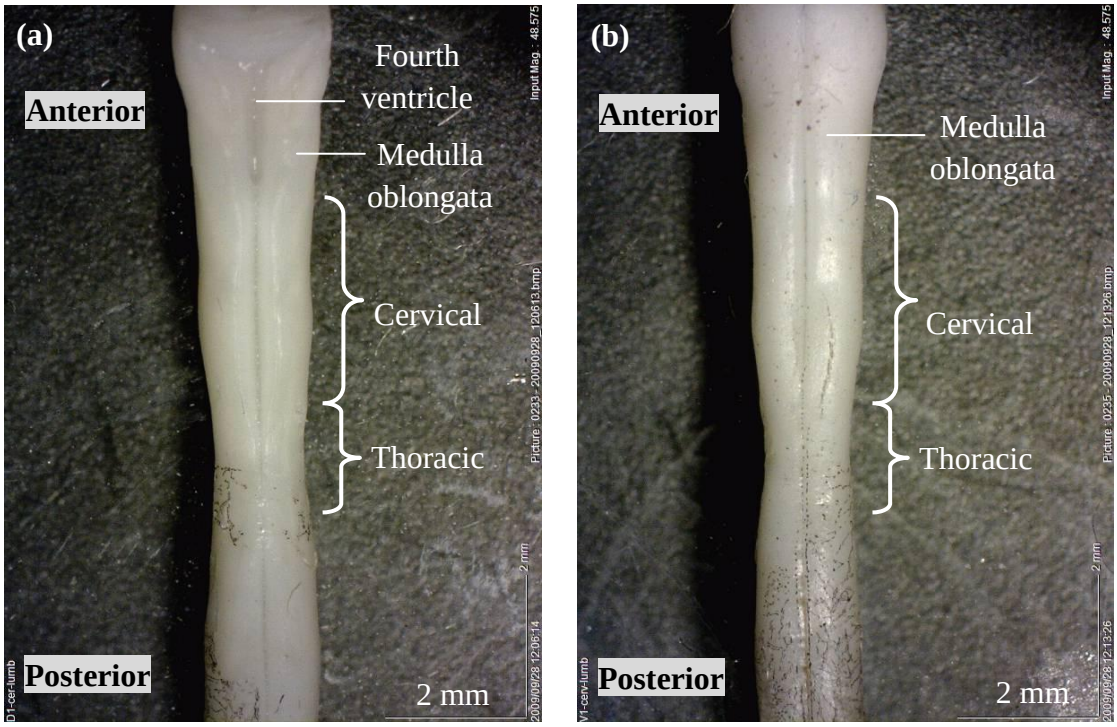

Figure 3.4: Rostral/anterior portion of the frog spinal cord; (a) dorsal view, (b) ventral view

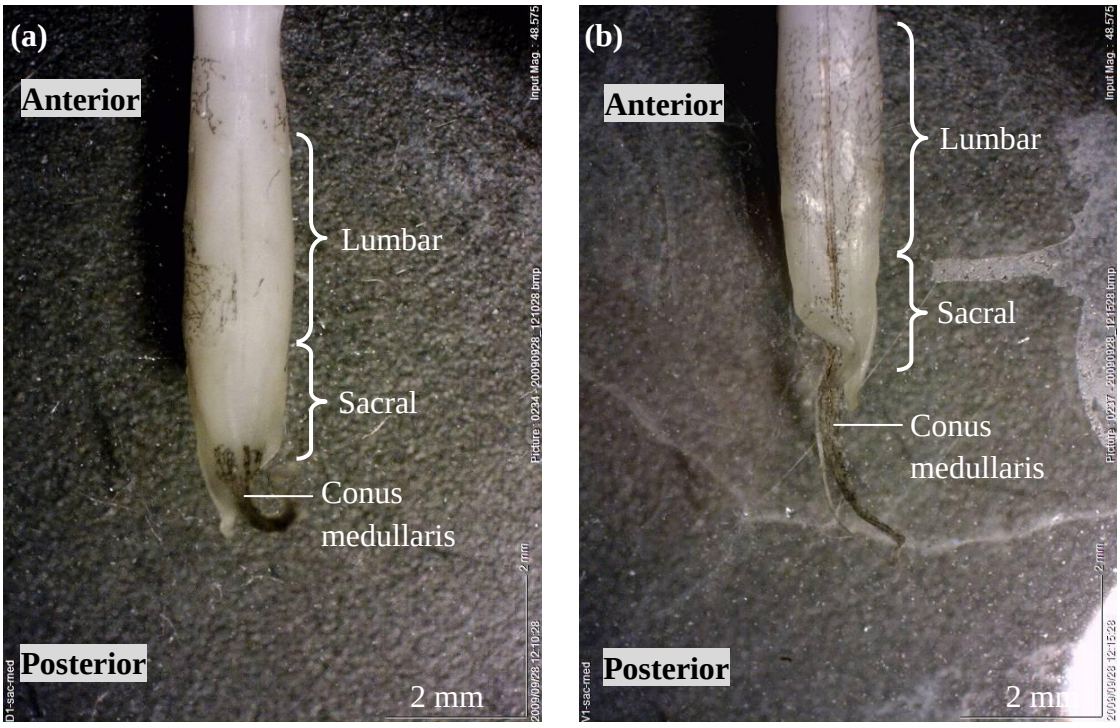

Figure 3.5: Caudal/posterior portion of the frog spinal cord; (a) dorsal view, (b) ventral

3.1.1 Morphometric Analysis of Specimen and its Spinal Cord

From the records of thirty adult frogs, their weights were in the range of 11–17 gram, with snout-to-vent length measured at 52–61 mm. The average weight and snout-to-vent length of the animals were 13.22 ± 1.62 g and 57.67 ± 3.28 mm, respectively (Table 2.3.1). In comparison, measurement data were also taken for their spinal cords after removal from the vertebral columns. The weight and average length of the spinal cord from these reported specimens were 0.034 ± 0.00 g and 11.58 ± 0.86 mm, respectively. From these values, the ratio of body weight to spinal cord weight and the ratio of body length to spinal cord length were generated as approximately 389:1 and 5:1, respectively.

The average length of each segmental region from rostral to caudal of the spinal cord, namely cervical, thoracic, lumbar and sacral were 3.56 ± 0.42 mm, 2.46 ± 0.28 mm, 3.44 ± 0.45 mm and 2.11 ± 0.33 mm, respectively. The cervical level was relatively longer than the other three, followed by the lumbar, sacral and thoracic levels. The guidelines for measurement taking in this morphometric analysis could be referred in Appendix A.

Table 3.1: Measurement data (mean ± standard deviation) of 30 adult frogs and their spinal cords.

	Parameter/Variable	***Mean ± Standard deviation***
Animal	Snout-to-vent length *(mm)*	57.67 ± 3.28
	Weight *(g)*	13.22 ± 1.62
Spinal cord	Length of cervical level *(mm)*	3.56 ± 0.42
	Length of thoracic level *(mm)*	2.46 ± 0.28
	Length of lumbar level *(mm)*	3.44 ± 0.45
	Length of sacral level *(mm)*	2.11 ± 0.33
	Total length *(mm)*	11.58 ± 0.86
	Weight *(g)*	0.034 ± 0.00

3.2 Histology of Frog Spinal Cord

Five types of staining methods namely the H&E, Nissl, Lillie's Variant of the Weil-Weigert, Thionin and modification of Golgi methods, that were used in this part of the work enabled the visualisation of different structures of the spinal cord possible (Figure 3.6). H&E was a basic histological staining method that showed the overall frog spinal cord organisation, highlighting the purple nuclei and pink cytoplasm. Nissl staining allowed the labeling of cell bodies in blue. Both H&E and Nissl methods outlined the morphologies of cell bodies but were unable to reveal the differentiation between grey and white matters. Lillie's Variant of the Weil-Weigert and Thionin, on the other hand, gave a clearer delineation of the grey and white matters as the axonal myelin sheaths were distinguished in contrasting colours. With the modification of Golgi method, the entire neuron including its processes appeared as a darkened element. This preparation did not consistently stain all neurons present in the spinal cord section when compared to the adjacent sections that were stained in other methods.

A transverse or cross section of the frog spinal cord (Figure 3.7, Figure 3.8) revealed a typical configuration with an inner core grey matter that surrounded a central canal and an outer white matter enveloping the grey. Lining the central canal was a cellular layer of ependymal cells. The grey matter, resembling the shape of a butterfly, was made up of dorsal and ventral horns in pairs. Lying in between these horns was a region known as the intermediate zone. The separating borders among them were, however, not precisely defined. In the white matter, it was organised into dorsal, lateral and ventral columns or funiculi. The left and right portions of the bilaterally symmetrical semi-bilobed structure were clearly separated by the anterior median fissure and posterior median sulcus. In representative transverse sections of each spinal segmental level, i.e.

cervical, thoracic, lumbar and sacral, the internal features differed from one another. Their differences are further explained in the later subchapters.

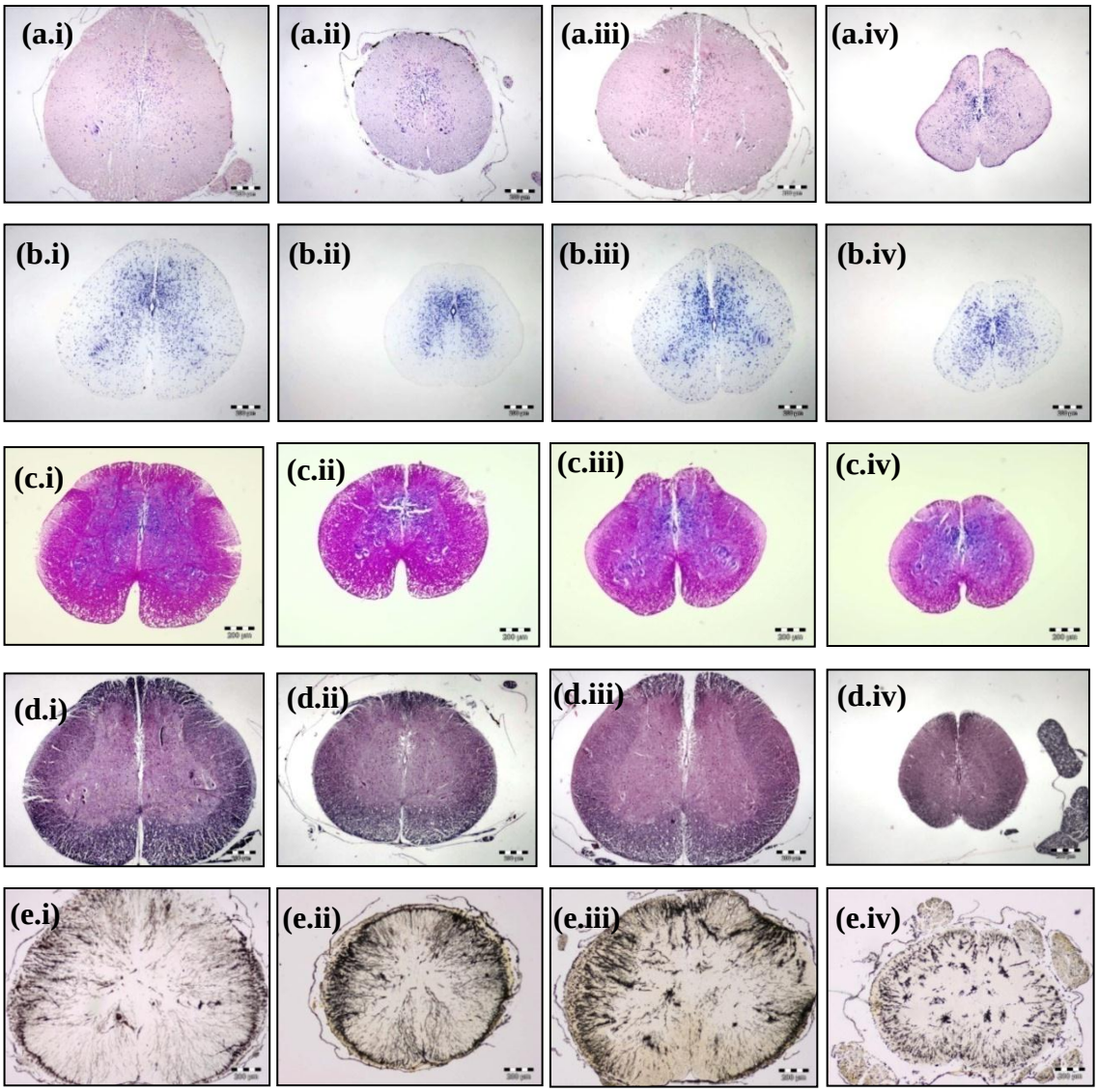

Figure 3.6: Index of representative spinal cord sections at four major levels; (i) cervical, (ii) thoracic, (iii) lumbar and (iii) sacral, stained in different histological staining methods; (a) H&E, (b) Nissl, (c) Thionin, (d) Lillie's Variant of the Weil-Weigert and (e) modification of Golgi (40× magnification).

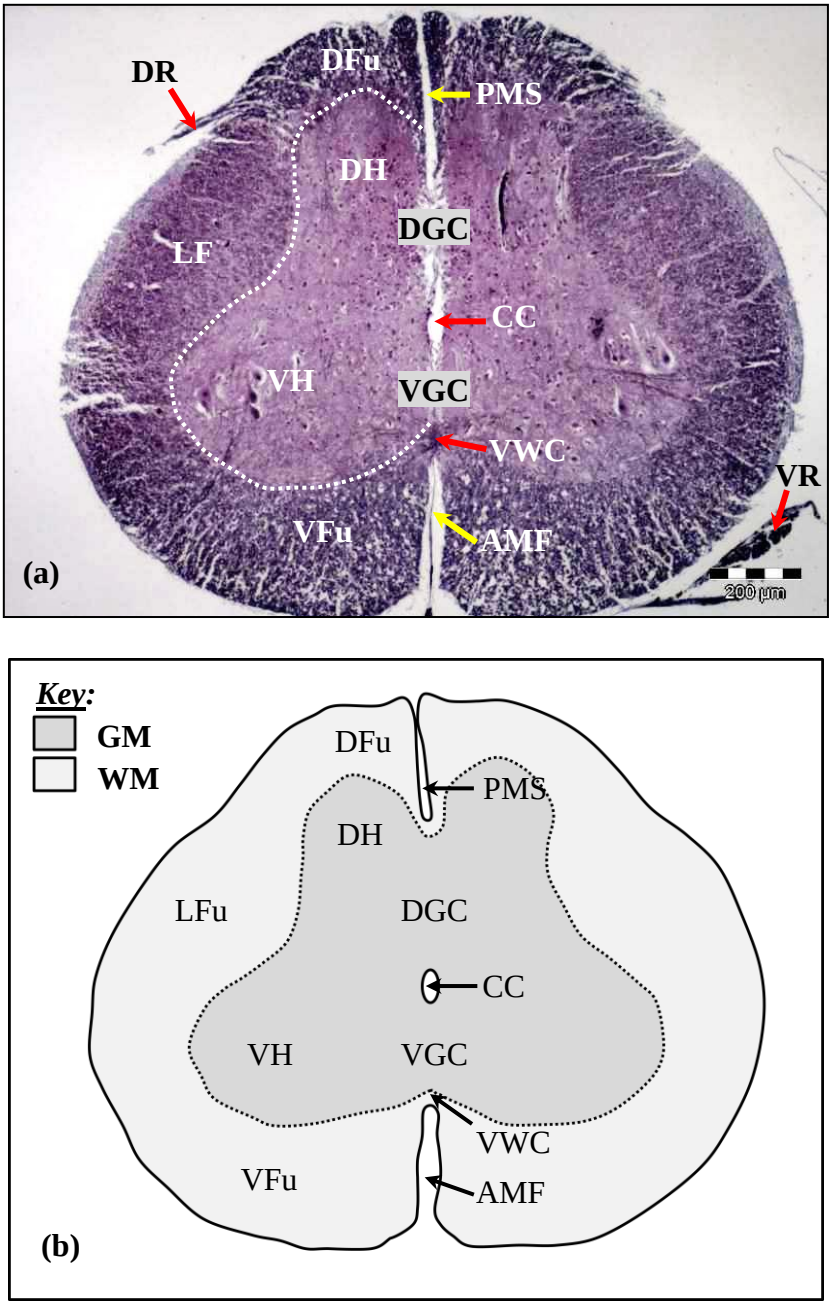

Figure 3.7: (a) Transverse section of frog cervical spinal segment stained with Lillie's Variant of the Weil-Weigert (40× magnification). Dotted line depicts the presumable boundary between the grey matter and white matter. (b) Diagrammatic representation of transverse section of frog spinal cord.

[AMF: anterior median fissure, CC: central canal, DFu: dorsal funiculus, DGC: dorsal grey commissure, DH: dorsal horn, DR: dorsal root of spinal nerve, GM: Grey matter, LFu: lateral funiculus, PMS: posterior median sulcus, VFu: ventral funiculus, VGC: ventral grey commissure, VH: ventral horn, VR: ventral root of spinal nerve, VWC: ventral white commissure, WM: White matter]

3.2.1 Histomorphometric Analysis of Spinal Segments

Quantitative measurement data of representative spinal cord segments recorded were inclusive of transverse and vertical diameters. Transverse diameter was described as the diameter of a spinal segment measured crosswise whereas vertical diameter was measured from an upright plane (Figure 3.8). Also noted in this analysis are the areas of the overall spinal segment cross section as well as the areas for both grey and white matters. These areas were measured using the mentioned software by outlining the presumable perimeters of the entire structure or specifically the grey or white matters. However, it is important to acknowledge the possibility that the recorded data might be underestimated or smaller than the actual value as the spinal cord tissue may have shrunk during histological procedures (Rolls, 2012).

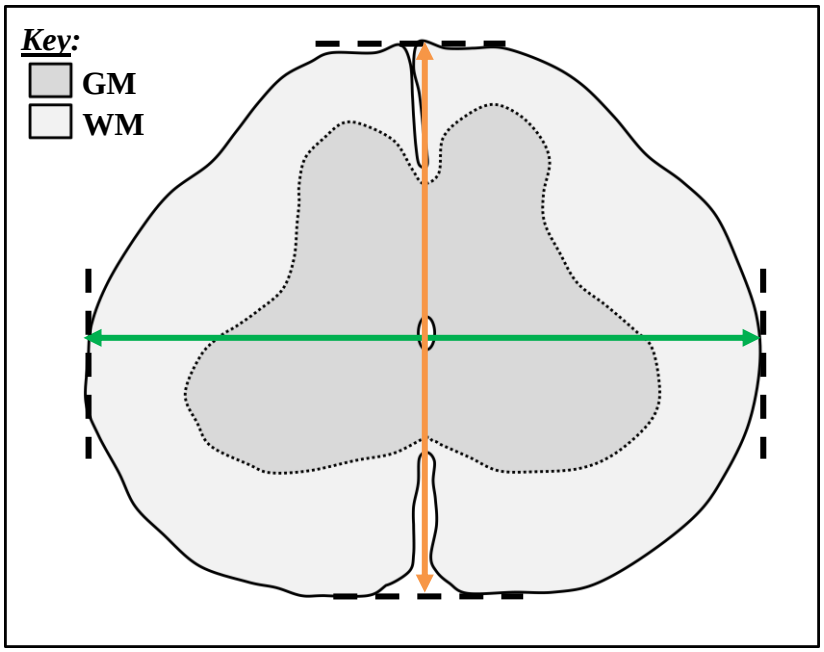

↔	Transverse diameter
↔	Vertical diameter

Figure 3.8: Guideline for measuring transverse and vertical diameters of the spinal cord transverse section.

Table 3.2: Diameter and the area of overall cross section of four representative spinal cord segments in six specimens in mean and standard deviation (mean ± SD).

No	Segmental level	Diameter *(Mean ± SD)*		Area of overall cross section *(mm^2)*
		Transverse diameter *(mm)*	Vertical diameter *(mm)*	
1.	Cervical	1.45 ± 0.07	1.26 ± 0.05	1.44 ± 0.09
2.	Thoracic	1.19 ± 0.05	1.00 ± 0.04	0.95 ± 0.06
3.	Lumbar	1.35 ± 0.10	1.15 ± 0.06	1.23 ± 0.09
4.	Sacral	1.13 ± 0.02	0.92 ± 0.04	0.74 ± 0.03

Table 3.3: Area measurements of grey matter and white matter in four representative spinal cord segments in six specimens in mean and standard deviation (mean ± SD).

No	Segmental level	Area *(Mean ± S.D.)*	
		Grey matter *(mm^2)*	White matter *(mm^2)*
1.	Cervical	0.58 ± 0.05	0.86 ± 0.06
2.	Thoracic	0.33 ± 0.02	0.62 ± 0.06
3.	Lumbar	0.52 ± 0.05	0.72 ± 0.05
4.	Sacral	0.31 ± 0.01	0.43 ± 0.02

According to Table 3.2, the cervical segment exhibited the biggest transverse and vertical diameters. This was closely followed by spinal segment from lumbar, thoracic and sacral regions. Similarly in Table 3.3, the overall cross-sectional area and the areas of grey and white matters were also found to be greater in the cervical and lumbar regions where enlargements of the structure were earlier reported. The thoracic and sacral levels showed a fair reduction in all of these areas. It could be therefore summarised that the diameter of a spinal segment is in proportion to its overall area. On the whole, the spinal cord showed a gradual decrease in diameter and area as its length descended from cervical to sacral, with a sudden increase in the lumbar level due to the enlargement as observed in its gross morphology (Table 3.2).

3.2.2 Grey Matter

As mentioned earlier, grey matter of the frog spinal cord transverse sections resembled the shape of two paired wings, which were noticeably separated into left and right halves. The upper portion made up the dorsal horns and they were composed of neurons that concerned with sensory processing. For the ventral horns, they took form of the lower portion of the grey matter, which contained motor neurons that innervated the skeletal muscles. Joining the left and right portions of the spinal grey were the dorsal and ventral commissures (Figure 3.9, Figure 3.10). These regions allowed nerve decussation or the crossing of nerve impulses from one side of the body to the other (Noble, 1954). The central canal was located at the centre of the spinal grey. This fluid-filled cavity was found along the length of the spinal cord with ependymal cells lining the walls of the canal.

The spinal grey mass contained a great concentration of cells with intermixed content of neuronal and glial cells. It appeared dense due to its major composition of neuronal cell bodies and their dendrites, as well as the unmyelinated axons. The latter were left unstained in the H&E and Nissl staining. From the stained sections, neuronal cell bodies were differentiated as to having light-coloured nuclear appearance, with the surrounding cytoplasm characterised into various shapes. These neuronal profiles are discussed in detail in subchapter 3.3. The ventral horns contained groups of larger neurons, which were presumably motor neurons (Figure 3.11, Figure 3.12). At the cervical and lumbar spinal regions, there were higher distributions of motor neurons residing in the ventral horn.

Apart from neurons, the second major cell population in the spinal grey were the supporting glial cells or neuroglia. Four types of neuroglia were found vastly among the

neuronal somas and visibly apparent in Nissl-stained sections (Figure 3.13). Their descriptions, as similarly mentioned by Stensaas and Stensaas (1967), were based on the stained cell bodies with no visible processes. Astrocytes were relatively large with somatal dimension (in width and length) of 5–7µm × 6–8µm, oval or sometimes irregularly shaped and had speckled appearance. Oligodendrocytes, the second type being identified, were smaller (3–5µm × 4–5µm) in comparison to the former type, spherically shaped and often seen as dense, darkly stained spots. For microglia, they appeared as small (3–4µm × 7–10µm), angular pellets. The dark and elongated ependymal cells (3–4µm × 5–7µm) that lined the area around the central canal, were also known to be one of the glial cells (Figure 3.14). In terms of size, glial cells were comparably smaller but often appeared to be more densely stained compared to neurons.

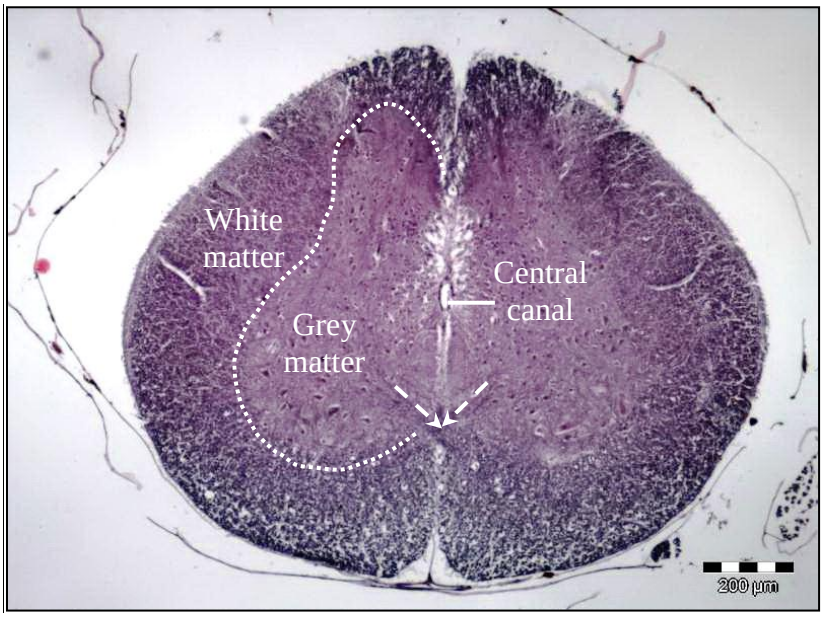

Figure 3.9: Transverse section of frog thoracic spinal segment, showing nerve decussation (as indicated by the arrows) at the ventral grey commissure (Lillie's Variant of the Weil-Weigert, 40× magnification)

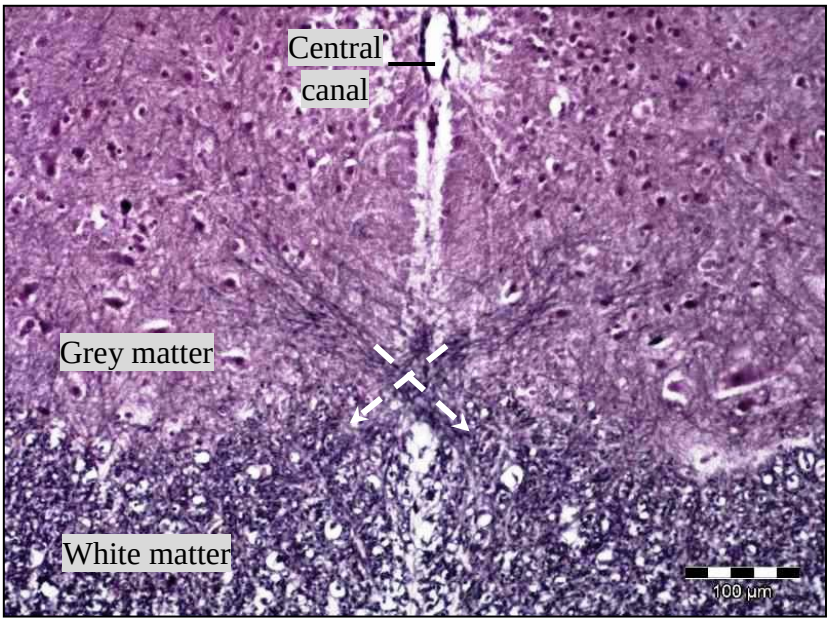

Figure 3.10: Nerve decussation (as indicated by the arrows) at the ventral grey commissure (Lillie Variant's of the Weil-Weigert, 100× magnification)

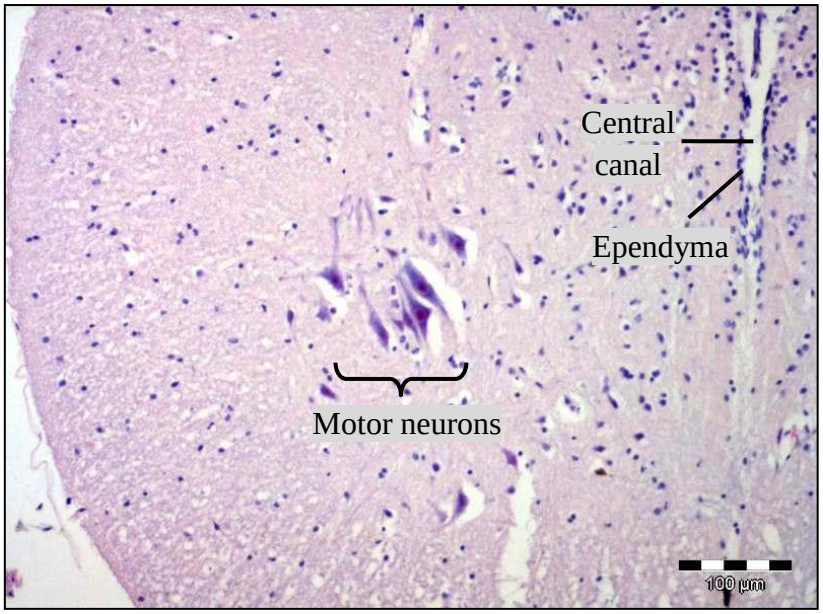

Figure 3.11: Motor neurons at the ventral horn (H&E, 100× magnification)

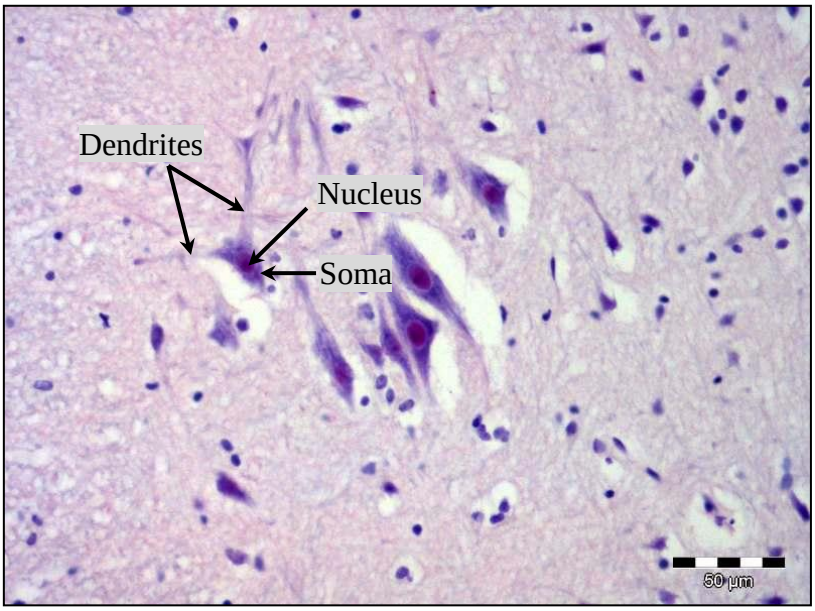

Figure 3.12: Motor neurons (H&E, 200× magnification)

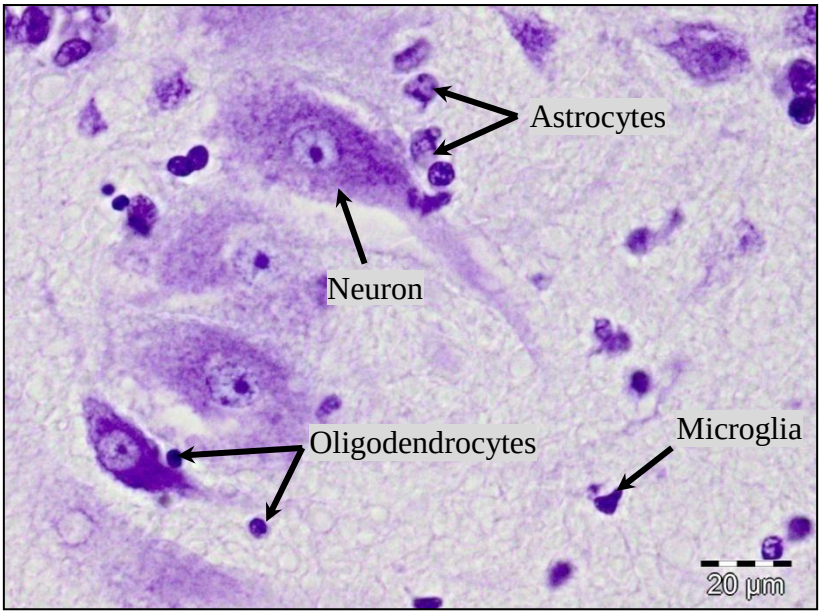

Figure 3.13: Neuron and neuroglia in the spinal cord grey matter (Nissl, 200× magnification).

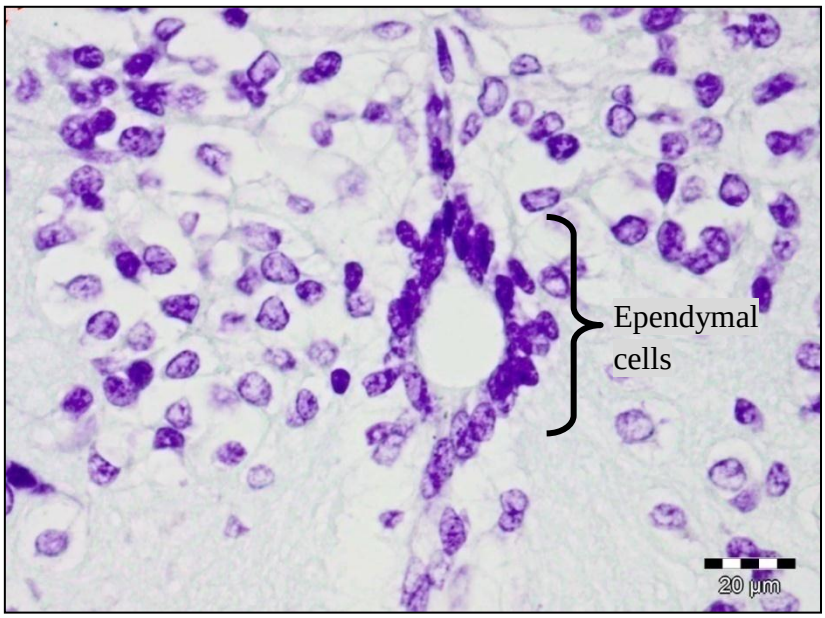

Figure 3.14: Ependymal cells lining the central canal (Nissl, 200× magnification).

3.2.3 White Matter

White matter contained bundles of myelinated axons of the ascending and descending tracts that lie longitudinally along the cord. Rostrally, these tracts could originate from the brainstem and other parts of the brain, thus allowing communication between the brain and the spinal cord. In the stained cross section using the Lillie's Variant of the Weil-Weigert staining technique, this portion could be clearly observed as dark violet masses, enveloping the lighter shade of purple that represented the grey matter (Figure 3.15). The density contrast hence, enabled the boundary that separated the white matter from the spinal grey to be fairly outlined. The stained white matter also showed foamy or vacuolated appearance.

The white matter was organised into three columns or funiculi; dorsal, lateral and ventral on each side. Dorsal funiculus was located laterally to the dorsal horn and posterior median sulcus while ventral funiculus lies laterally to the anterior median fissure and below the ventral horn of the grey matter. The area connecting the dorsal and ventral funiculi was identified as lateral funiculus. Below the ventral grey

commissure, the ventral commissure of the white was found, which seemingly connects the two symmetrical halves of the spinal cord.

This outer region showed the absence of neuronal cell bodies. With thionin method, the bluish stained small cells indicated the non-neuronal glial cells, which were dispersedly distributed in the white matter (Figure 3.16). Although the refined details of the glial cells were rather inconspicuous, yet the different types could still be distinguished based on the characteristics as stated previously for Nissl-stained sections. Also observed in the cross section of the white matter were the myelinated nerve cell axons.

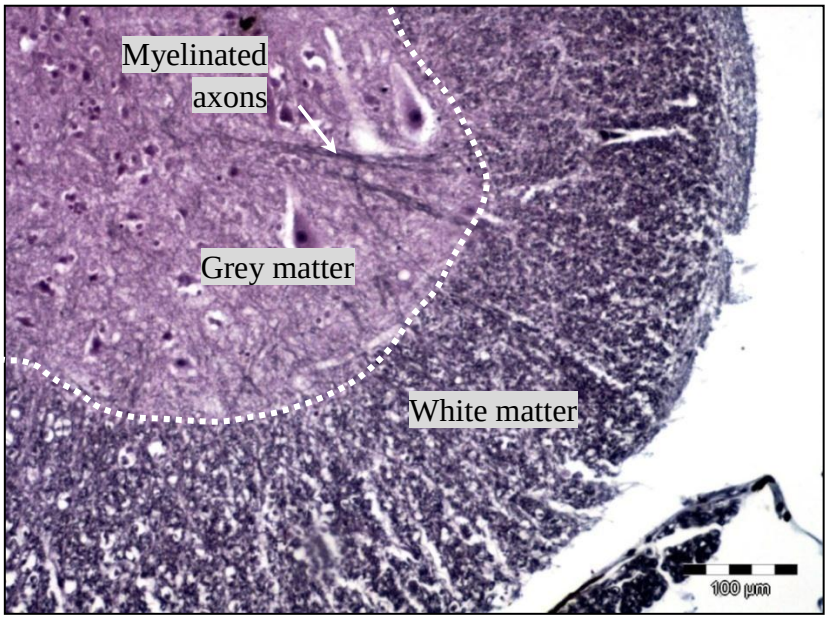

Figure 3.15: Grey and white matter segregation (with myelinated axons running across the grey) in a transverse section of a frog spinal cord (Lillie's Variant of the Weil-Weigert, 100× magnification)

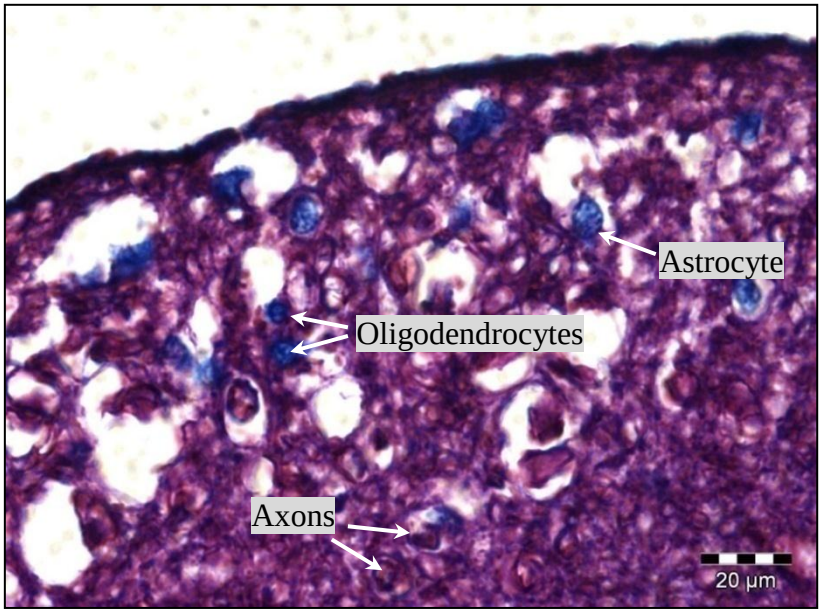

Figure 3.16: Spinal cord white matter (Thionin, 400× magnification)

3.3 Cytoarchitecture of Frog Spinal Grey

In this study, even with all the staining techniques used, the spinal grey matter was still poorly differentiated into any form of groups or clusters, especially in the dorsal horn and intermediate zone. Hence, the organisation of the grey matter into the conventional nuclear groups and Rexed's laminae could only serve as reference or a comparative model in describing the cytoarchitecture of this region. Instead, an alternative demarcation scheme that divides the grey area into fields, as being put forward by Ebbesson (1976), was seemingly to be more appropriate. According to the Ebbeson's system, the spinal grey was divided into seven specific fields: dorsal field (DF), lateral field (LF), central field (CF), ventrolateral field (VLF), ventromedial field (VMF), lateral motor field (LMF), and medial motor field (MMF) (Figure 3.17). It is important to note that there were no distinct boundaries between each of the division or region, instead they are usually recognised as transitional zones. The organisation of spinal grey is to be discussed further in the following subchapters and the description of the mentioned fields is based mainly on the Nissl-stained material.

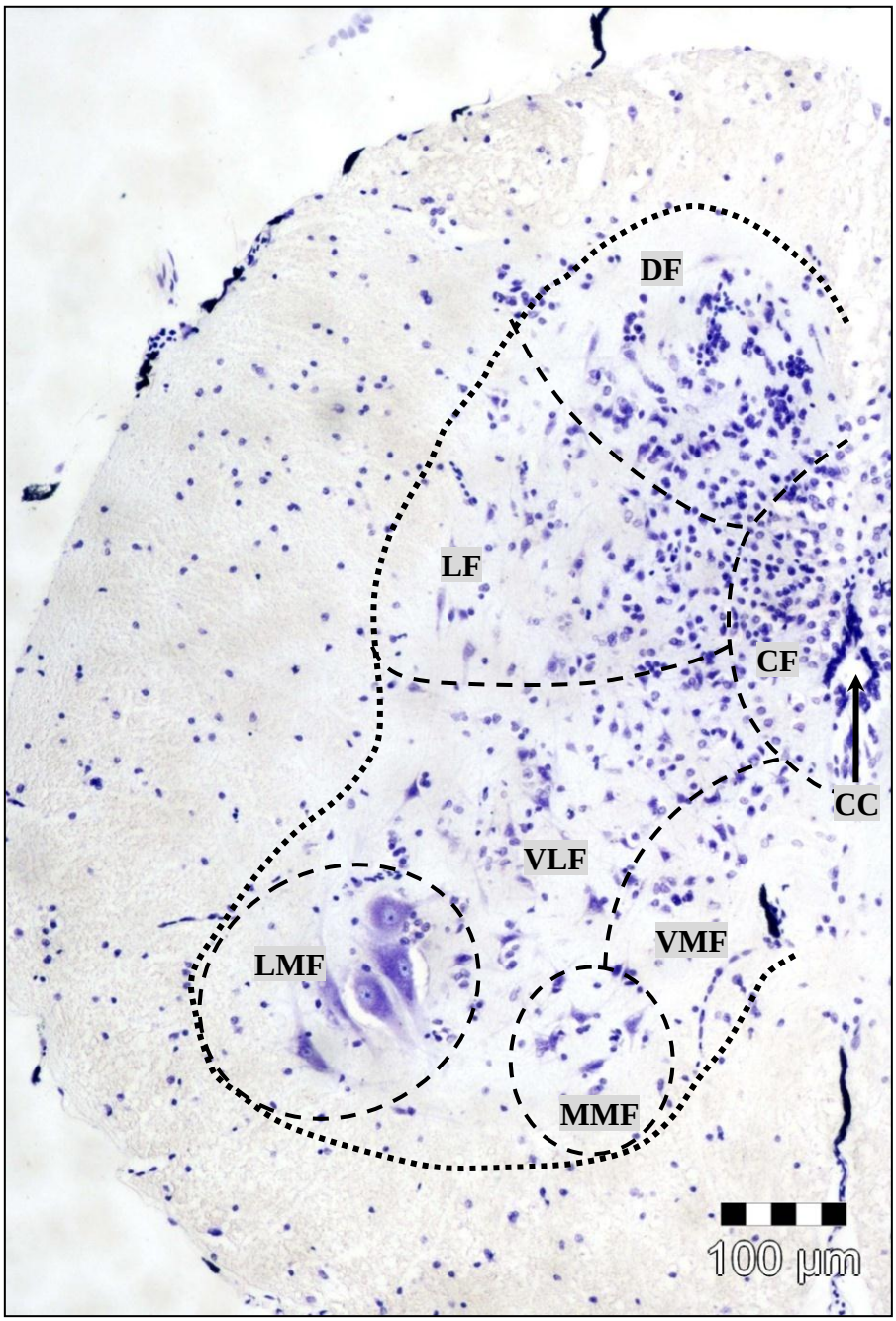

Figure 3.17: Nissl-stained lumbar section of the frog spinal cord with proposed cytoarchitectonic regions identified based on modification of Ebbeson's field system (100× magnification). [CC: central canal, CF: central field, DF: dorsal field, LF: lateral field, LMF: lateral motor field, MMF: medial motor field, VLF: ventrolateral field, VMF: ventromedial field]

3.3.1 Morphological Characterisation and Distribution of Neuronal Somas

Nissl and Golgi staining methods that were employed in the study helped in the visualisation of neuronal somas. Neuronal soma is the largest portion of a neuron that contained the nucleus and other organelles. Specialised extensions of the neuronal soma are called dendrites (which receive incoming electrochemical signals) and axon (which carries the signal away from the soma). Although the probability of having a complete neuron being included in the same plane of a section was very unlikely, the combination of both methods has allowed the morphological characterisation of the neuronal soma to be conducted.

Nissl staining method revealed the occurrence of neuronal and non-neuronal cells in the frog spinal cord cross sections (Figure 3.17). The prominence of the dark blue stained structures, which highlighted the Nissl substance and nucleoli within the cell perikarya and the hollow space of the nuclei, hence enabled the observation and identification of neurons. Proximal part of dendritic processes found in the same plane as soma, were also normally stained.

In contrast, Golgi staining method allowed the expression of only a few selected neuronal cells in their entirety. The demonstration of an individual neuronal cell body and its processes in a Golgi-stained section was represented as dark brown to black masses. The surrounding tissue was completely unstained, remaining as obscure as the transparent, dull yellowish background. The underlying reason for the capricious results is still unknown (Cullen, 2009). Also, the total course of the dendritic arborisation of neurons were often non-continuous or appeared to end and resurface abruptly as they might have been cut during sectioning (Figure 3.18).

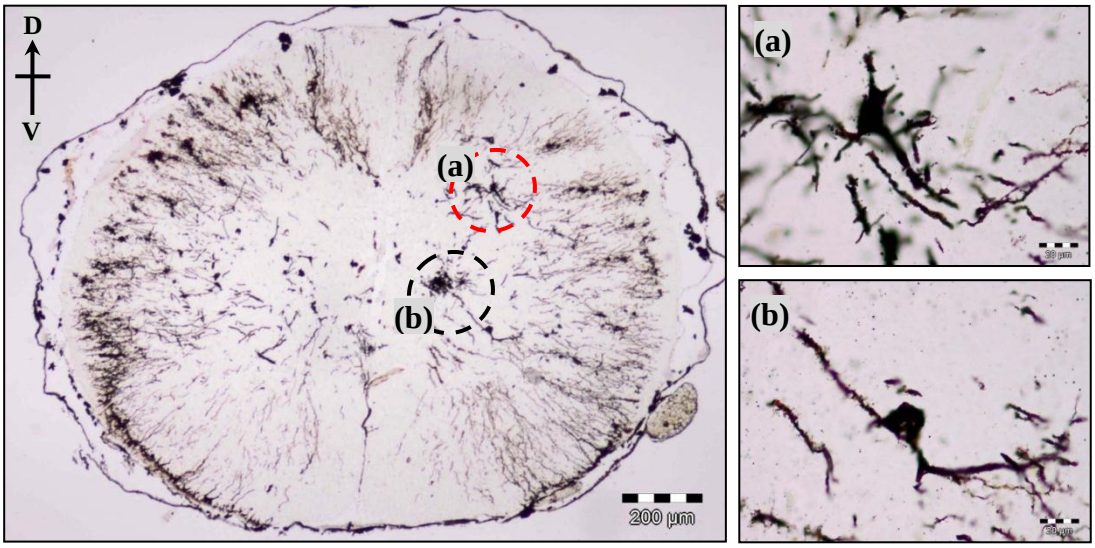

Figure 3.18: Golgi-stained cervical spinal section (40× magnification). Insets showed the neuronal profiles from (a) dorsal horn and (b) ventral horn, with incomplete projection of processes (400× magnification). [D: dorsal, V: ventral]

The spinal grey was morphologically heterogenous, with somas differing in shape and size. In this study, neuronal cell type profiles were distinguished based on: (a) size of soma, (b) shape of perikarya, (c) number of main processes extending from the cell body, as well as (d) the location where they were found. The analysed cells were summarised into four major shapes, as similarly reported in cats (Galhardo and Lima, 1999), monkeys (Tashiro et al., 1990) and elesmobranch fishes (Cameron et al., 1990) ; (a) spindle, (b) triangular, (c) polygonal, (d) tear. Neurons with spindle-shaped somata were characterised by two primary processes arising from the opposite poles of the tapering ends. Second group of cells was shown to have triangular or pyramidal somatal shape and its major arbors extended from each of the corners. As for the polygonal-shaped somata, there were four or more primary processes arising from the somatal corner. Some neurons were recognised by the tear shape of the cell bodies, where a singular arbor protruded at the pointed tip. In addition, there were also other somatal shapes present among the groups as described, such as round, ovoid and some with indeterminate forms. However, they occurred in a relatively small number. All the mentioned profiles were adaptable for cells in all fields of the frog spinal grey. The

variety of somatal shape morphologies are represented in the photomicrographs as shown in Figure 3.19, Figure 3.20 and Figure 3.21.

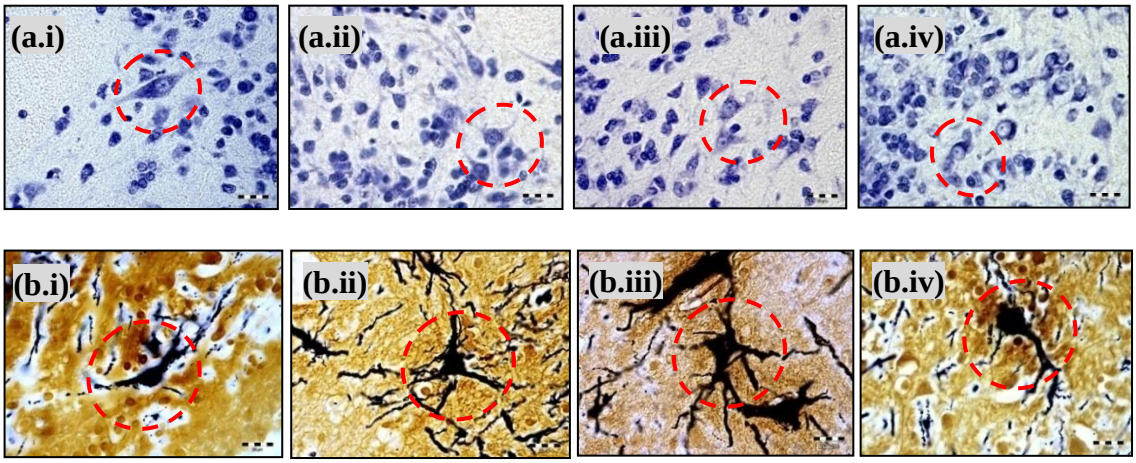

Figure 3.19: Varied examples of major neuronal soma morphologies in the dorsal and lateral fields; (i) spindle, (ii) pyramidal (iii) polygonal and (iv) tear, stained in (a) Nissl (and (b) modification of Golgi method (400× magnification).

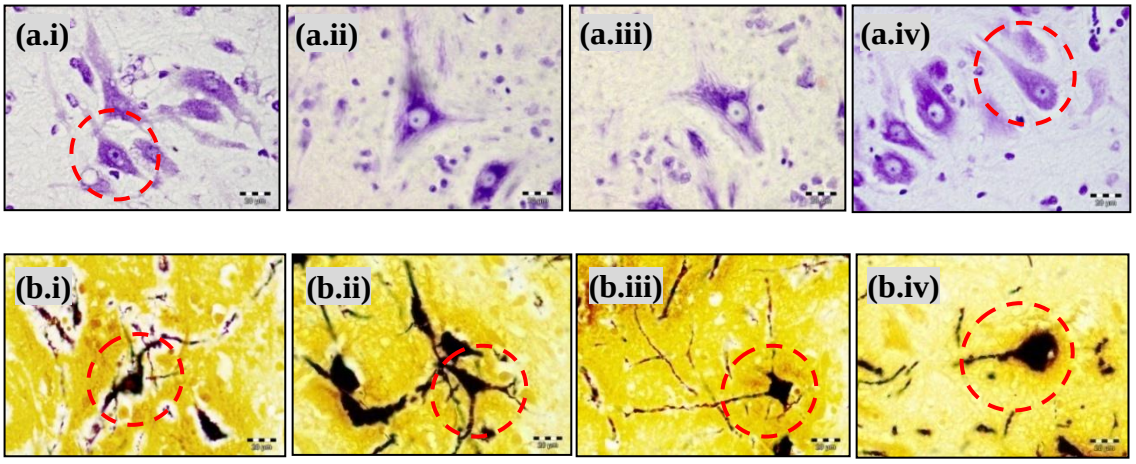

Figure 3.20: Varied examples of major neuronal soma morphologies in fields of the ventral horn; (i) spindle, (ii) pyramidal (iii) polygonal and (iv) tear, stained in (a) Nissl and (b) modification of Golgi method (400× magnification).

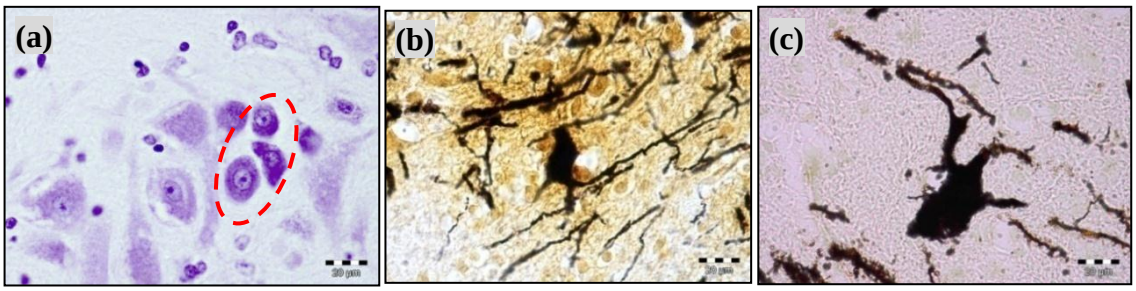

Figure 3.21: Varied examples of other neuronal soma morphologies; (a) round-to-ovoid (Nissl, 400× magnification) and (b)-(c) indeterminate shapes (modification of Golgi, 400× magnification).

Within 100µm thickness of each representative segmental level of the frog spinal cord from 6 adult specimens (n=6), a total of 1020 identifiable neuronal cell bodies, with mean cell number of 169.99, were recorded (Table 3.4, Figure 3.22). On average, there were 44.90% of the cells in spindle shape, 29.40% in triangular shape, 11.08% having polygonal shape and 7.65% in tear shape. Only about 6.67% of the cells were showing other miscellaneous forms. From the one-way ANOVA test conducted on the data, the numbers of recorded somas differed significantly ($p<0.05$) among the five somatal shapes (Appendix F).

Throughout the length of the spinal cord, neuronal cell occurrence was highest in cervical segmental level (36.27%), followed by lumbar and thoracic sections, which showed an almost comparable percentage number of cells (24.71% and 23.43%, respectively), while sacral spinal segments showed the lowest occurrence (15.59%) amongst them (Table 3.5, Figure 3.23). There was a statistically significant difference ($p<0.05$) in the numbers of neuronal somas among the four segmental levels (Appendix F). The relative distribution pattern of each somatal shape was consistent across the segmental levels, with spindle-shaped neurons being most abundant, followed by those in triangular and polygonal forms. Variability in concentration between tear and other miscellaneous shapes was observed; however, it was deemed minor.

As for Ebbeson's specific parcellation of neuronal cells into fields, majority of the identifiable neuronal somas were located at the ventral horn. They were particularly found in the lateral motor field and medial motor field, 42.55% and 22.65% respectively, of the total cell being identified. The lateral field had higher neuronal population (17.06%) as compared to the loosely packed dorsal field (12.15%). Whereas for central field, ventrolateral and ventromedial fields, the neuronal cells were scarcely distributed and only composed of 0.49%, 3.24% and 1.86% from the total mean number of identified somas (Table 3.6, Figure 3.24). The numbers of recorded somas were significantly different ($p<0.05$) for the seven fields of spinal grey (Appendix F). From Figure 3.24, neuronal soma of spindle-like shape pre-dominated each of the investigated field all through the length of spinal cord, followed by triangular-shaped neurons. Other neuronal somas morphologies exhibited some fluctuations and the difference in relative proportions of these cells was seen across different fields. All of the investigated fields, with the exception of central field, appeared to have mixed population of neuronal cells in relation to their distinctive shapes.

The lateral motor field was also observed to be heavily concentrated with neurons especially at the cervical, lumbar and sacral spinal sections while most of them are pooled at the medial motor field for sections of the thoracic segments. For each dorsal field, lateral field, central field, ventrolateral field and ventromedial field, the proportion of neuronal somas occurred in a rather similar amount throughout the spinal cord levels (Table 3.7, Figure 3.25).

Table 3.4: Distribution of neuronal soma morphological types in the spinal grey of adult *Fejervarya limnocharis*.

Somatal shape	***Number of cells***	***Mean cell number***	***Percentage (%)***
Spindle	458	76.33	44.90
Triangular	303	50.50	29.70
Polygonal	113	18.83	11.08
Tear	78	13.00	7.65
Others	68	11.33	6.67
Total	1020	169.99	100.00

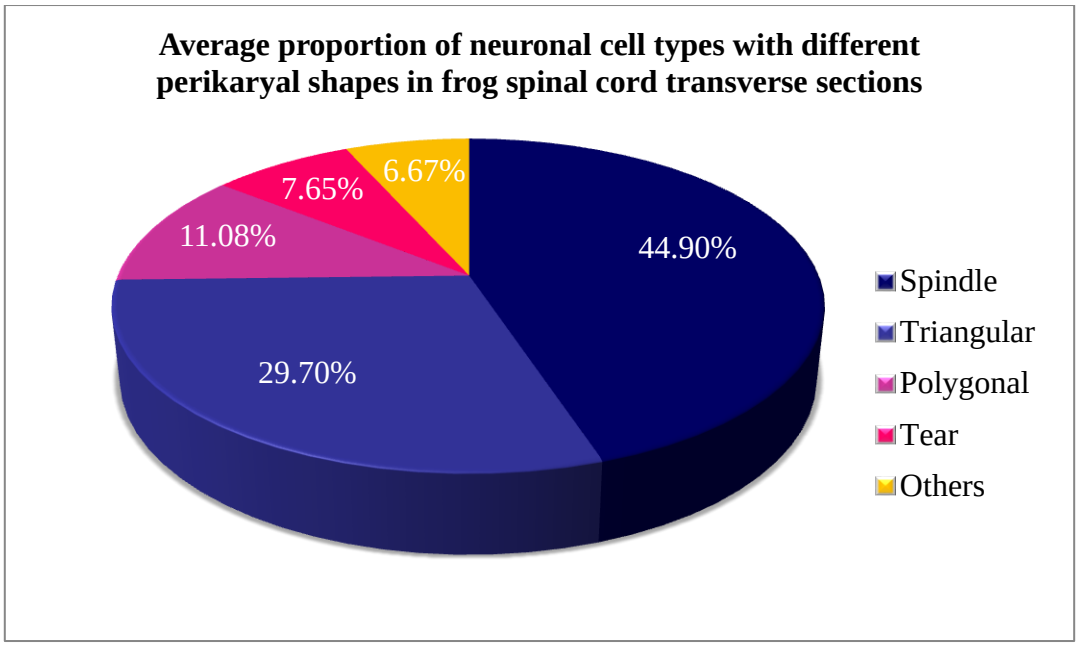

Figure 3.22: Pie chart displaying the average proportion of neuronal soma morphological types in frog spinal cord transverse sections.

Table 3.5: Average segmental proportion of neuronal soma morphological types in frog spinal cord transverse sections of adult *Fejervarya limnocharis*.

Segmental level	***Mean number of neuronal somatal shapes***					***Mean total***	***%***
	Spindle	***Triangular***	***Polygonal***	***Tear***	***Others***		
Cervical	25.17	18.83	6.33	5.50	5.83	61.66	36.27
Thoracic	17.33	11.83	4.33	3.17	3.17	39.83	23.43
Lumbar	21.00	12.67	5.33	1.83	1.17	42.00	24.71
Sacral	12.83	7.17	2.83	2.50	1.17	26.50	15.59
Mean total	76.33	50.50	18.82	13.00	11.34	169.99	-
%	44.90	29.40	11.08	7.65	6.67	100.00	100.00

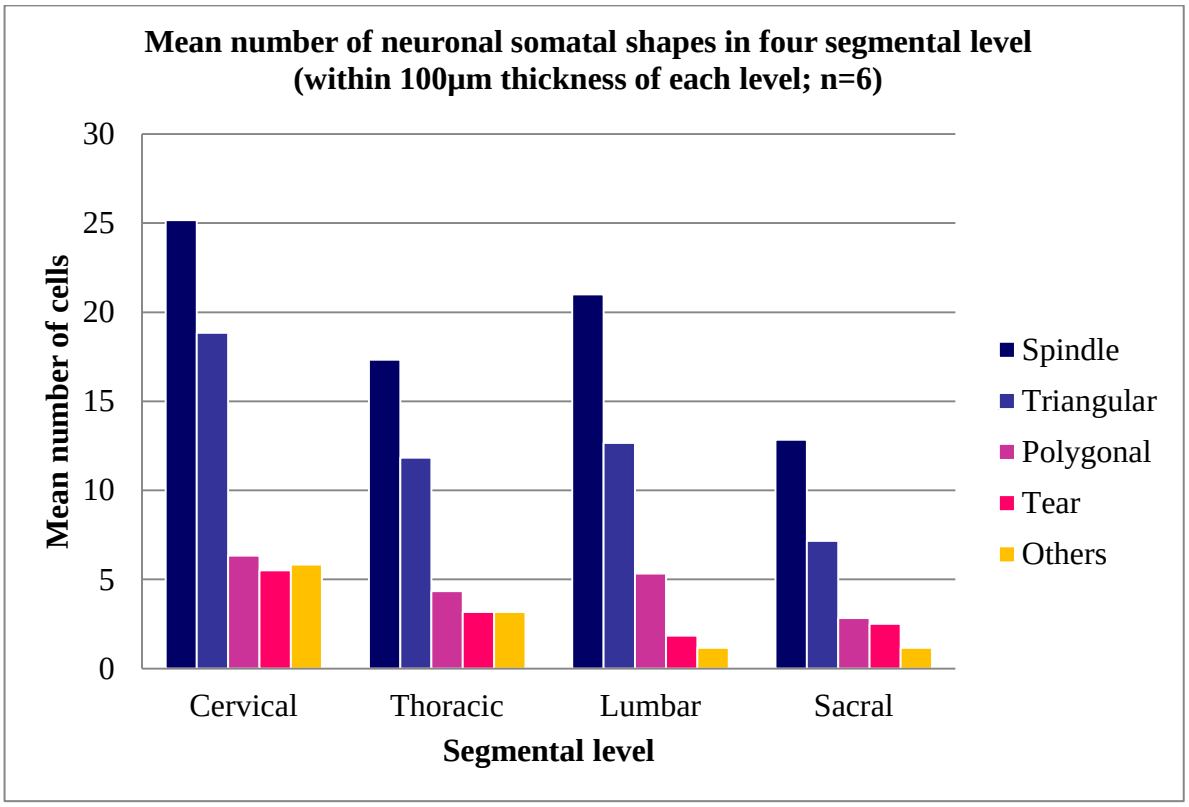

Figure 3.23: Histogram showing the distribution of neuronal soma morphological types in four spinal cord segmental levels.

Table 3.6: Average proportion of neuronal soma morphological types according to the major field segregation of the frog spinal cord transverse sections. [DF: dorsal field, LF: lateral field, CF: central field, LMF: lateral motor field, MMF: medial motor field, VLF: ventrolateral field, VMF: ventromedial field]

Somatal shape	***Mean number of neuronal somas in fields***						
	DF	**LF**	**CF**	**LMF**	**MMF**	**VLF**	**VMF**
Spindle	10.33	12.17	0.83	32.83	16.33	2.50	1.33
Triangular	9.33	10.50	0	17.00	10.00	2.50	1.17
Polygonal	0.50	3.17	0	8.17	6.50	0	0.50
Tear	0.33	1.67	0	7.67	3.00	0.17	0.17
Others	0.17	1.50	0	6.67	2.67	0.33	0
Mean total	20.66	29.01	0.83	72.34	38.50	5.50	3.17
%	12.15	17.06	0.49	42.55	22.65	3.24	1.86

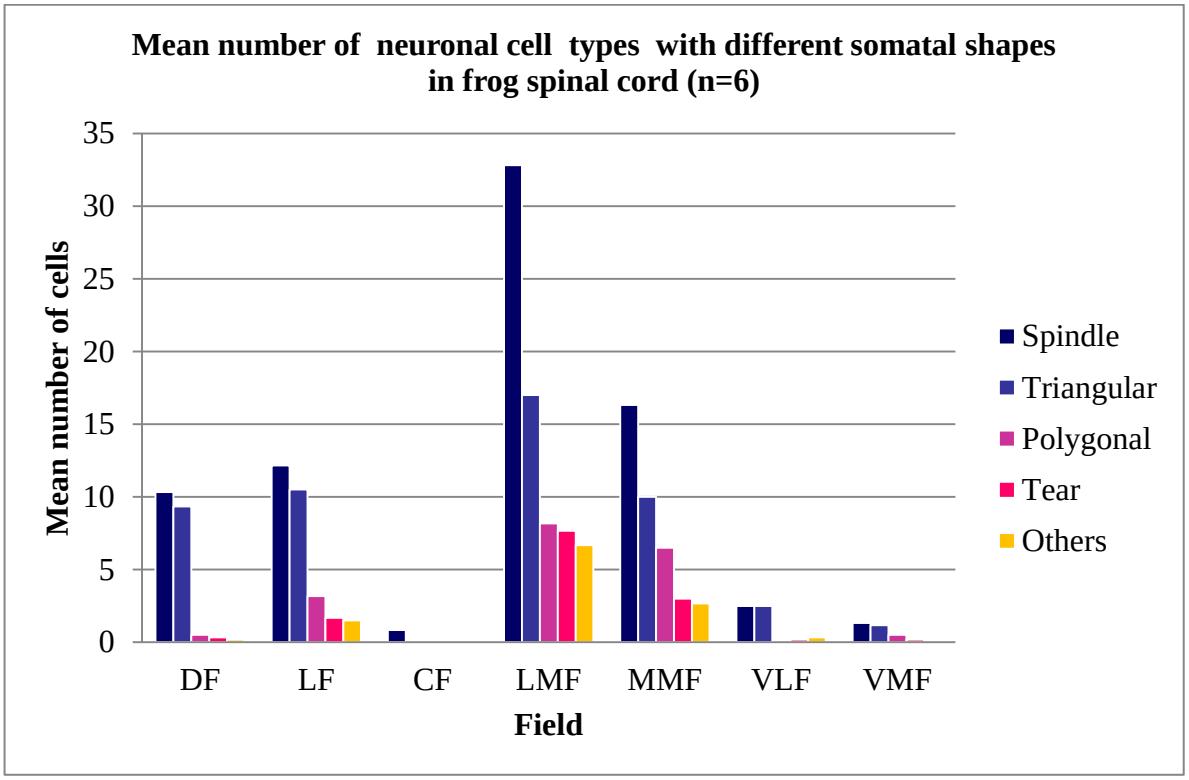

Figure 3.24: Histogram showing the distribution of neuronal soma morphological types in the major field segregation of the spinal cord transverse sections for six adult *Fejervarya limnocharis*. [DF: dorsal field, LF: lateral field, CF: central field, LMF: lateral motor field, MMF: medial motor field, VLF: ventrolateral field, VMF: ventromedial field]

Table 3.7: Average proportion of neuronal soma in different spinal grey fields at each of the spinal cord segmental levels. [DF: dorsal field, LF: lateral field, CF: central field, LMF: lateral motor field, MMF: medial motor field, VLF: ventrolateral field, VMF: ventromedial field]

Segmental level	***Mean number of neuronal somas in fields***							***Mean total***	***%***
	DF	**LF**	**CF**	**LMF**	**MMF**	**VLF**	**VMF**		
Cervical	6.67	9.33	0.17	33.83	9.00	2.17	0.50	61.66	36.27
Thoracic	6.67	8.5	0.33	5.50	16.83	1.00	1.00	39.83	23.43
Lumbar	5.83	9.17	0.17	20.16	4.00	1.67	1.00	42.00	24.71
Sacral	1.50	2.00	0.17	12.83	8.66	0.67	0.67	26.50	15.59
Mean total	20.66	29.01	0.83	72.34	38.50	5.50	3.17	169.99	-
%	12.15	17.06	0.49	42.55	22.65	3.24	1.86	-	100.00

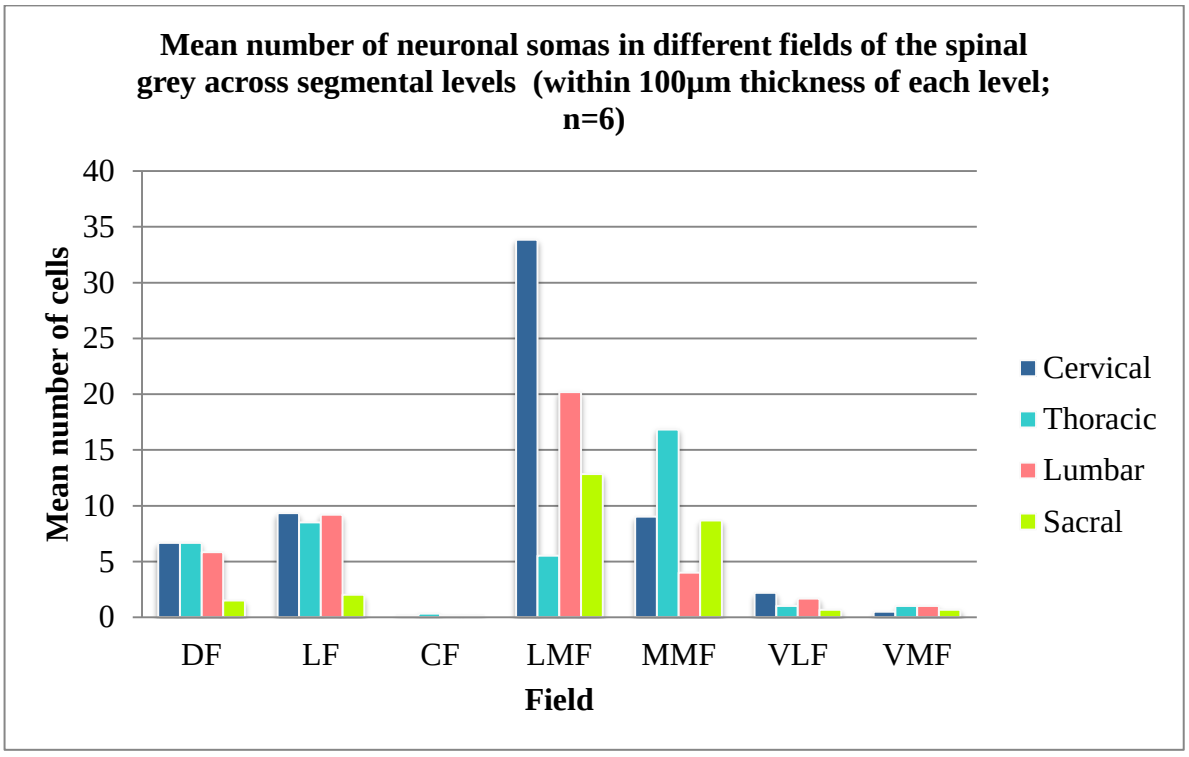

Figure 3.25: Histogram showing the distribution of neuronal soma in the major field segregation of the spinal segmental level for six adult *Fejervarya limnocharis*. [DF: dorsal field, LF: lateral field, CF: central field, LMF: lateral motor field, MMF: medial motor field, VLF: ventrolateral field, VMF: ventromedial field]

3.3.2 Dorsal Field

Dorsal field capped a big mass of the dorsal horn, which is the apex region of the grey matter. The dorsal horn was marked as the projection site of afferent dorsal root fibre, which appeared to form a network of nerves (Figure 3.26). The mean depth of this field was approximately 129–187µm from the dorsal grey matter border of a cross section. This field was loosely packed with mostly small-sized neurons and the supporting glial cells (Figure 3.27). Majority of the scattered neuronal somas were recognised as spindle and triangular in shape, whilst those in the form of polygonal and tear shapes occurred in small amount. The perikaryal dimensions, in width and length, of the commonly seen neurons measured from 4–15µm × 12–44µm for spindle-like cells and 8–19µm × 8–34µm for triangular shaped cells (Table 3.8).

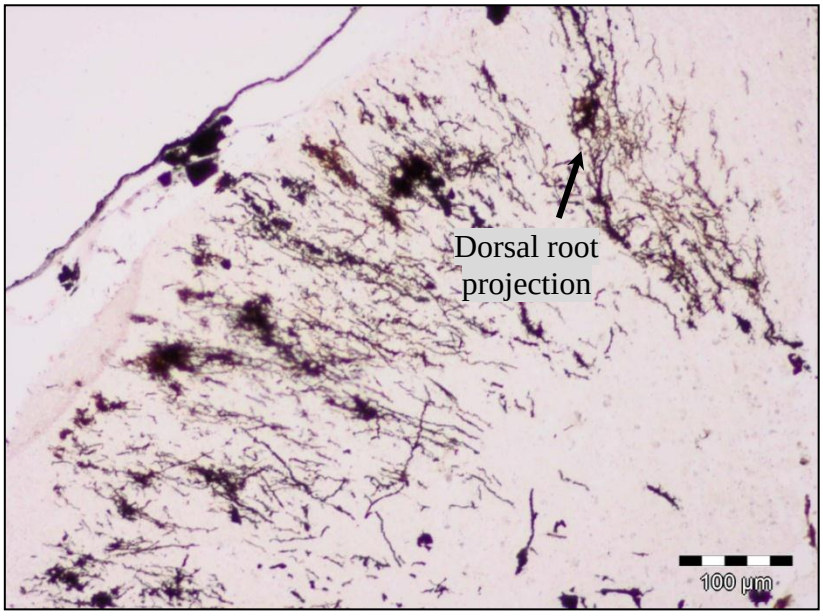

Figure 3.26: Incoming dorsal root fibres into the dorsal field (modification of Golgi, 100× magnification).

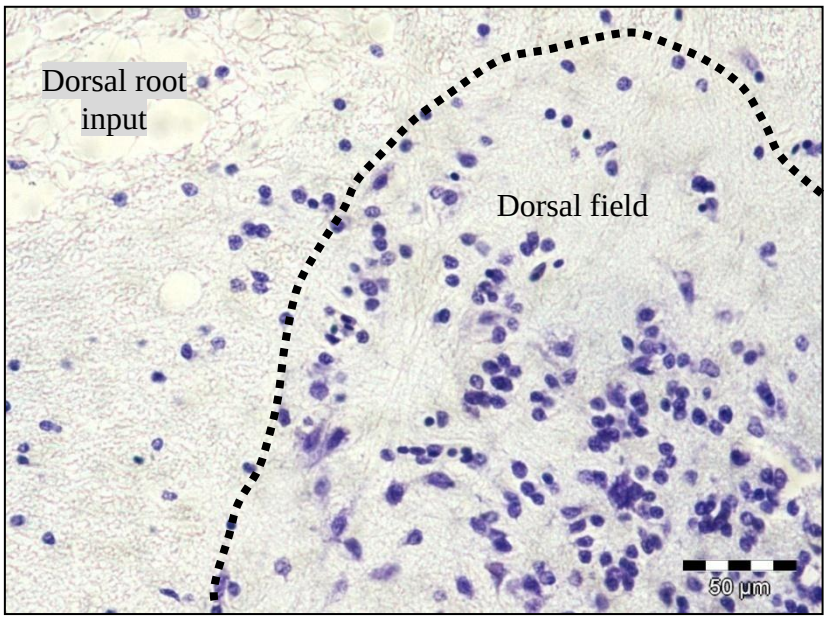

Figure 3.27: Dorsal field with loosely packed content (Nissl, 200× magnification).

3.3.3 Lateral Field

Lateral field encompassed the lower portion of the dorsal horn and a part of the intermediate grey area that stretched laterally to the anterior portion of the central field (Figure 3.28). From the basal edge of dorsal field, this region averagely extended 155–226µm vertically across the intermediate grey area and ended at the vague upper border of ventral field. Lateral field showed higher neuronal density and thus, a more compact organisation in comparison to the dorsal field. Similarly, neuronal cells of spindle-, triangular-, tear- and polygonal-shaped somas were found with the highest to lowest occurrence in the respective order. The size of the neuronal somas found were relatively comparable to those located in the dorsal field. The perikaryal dimensions ranged from, in width and length, 6–15µm × 15–42µm for spindle shaped somas, 5–23µm × 8–27µm for triangular somas, 6–14 × 6–14µm for polygonal shaped somas and 6–12µm × 12–21µm for tear-like somas (Table 3.8).

This field could be divided into lateral zone and medial zones. Based on the observation of the cell diameter, the identified cells in the medial region were usually smaller and fewer compared to those at the lateral side, which consisted of a greater amount of larger cells, majority in spindle form, although they were more loosely distributed. Glial components also appeared lesser in the lateral zone than in the medial zone.

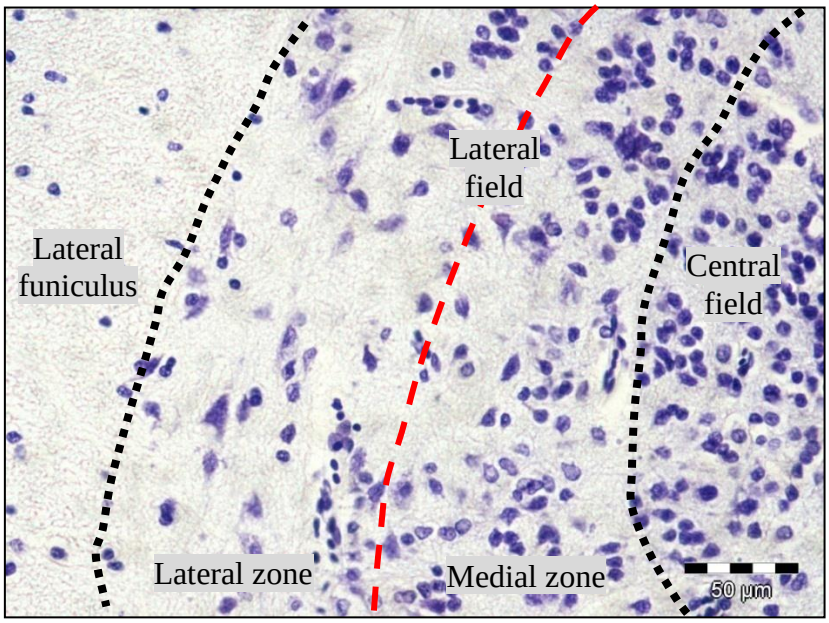

Figure 3.28: Location of lateral field (Nissl, 200× magnification).

3.3.4 Central Field

Central field represented the region surrounding the central canal, including the dorsal and ventral grey commissures. It was laid within 204–339µm around the perimeter of the central canal. This field appeared to have scant amount but mostly devoid of any recognisable neuronal somas. If located, these cell bodies were usually seen at the dorsal and medial areas of the central field rather than then ventral portion. The neuronal somas found appeared solely as spindle-shaped and usually positioned horizontally (Figure 3.29). They measured from 3–5µm wide, and 10–12µm lengthwise (Table 3.8). The central field was however, greatly concentrated with supporting glial cells, particularly ependymal cells that were found in abundance immediately lining the

central canal. The transition of glial cell density was evident as cells gradually increased in number from the lateral field to the central field.

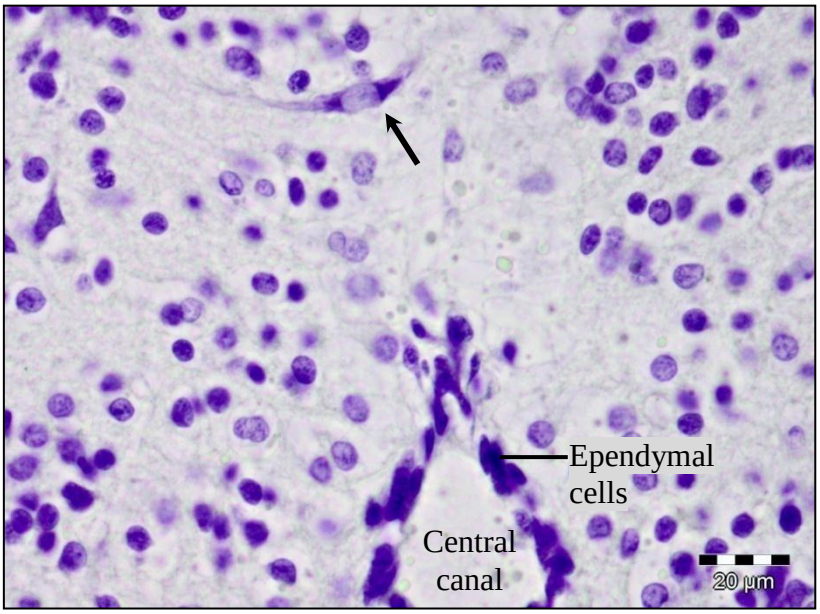

Figure 3.29: A spindle-shaped neuronal cell body (indicated by black arrow) found at the dorsal portion of central field (Nissl, 400× magnification).

3.3.5 Ventrolateral Field

In a transverse section, the remaining four fields of spinal cord including ventrolateral field, ventromedial field, lateral motor field and medial motor field, were vertically situated within 202–306µm from the ventral border of the grey matter. Ventrolateral field constituted the largest area within the grey matter, which corresponded to the intermediate zone and parts of the ventral horn (Figure 3.30, Figure 3.31). It borders on the lateral funiculus laterally and adjacent to the lower portion of the central field. Occurrence of somas with nuclei detected was low, with mean total of cell within 100µm thickness of 5.5 (Table 3.6, Figure 3.24). Also, they appeared more dispersed than in the lateral field. Mostly identified in this field were spindle and triangular somas. Their somatal size ranged from 8–20µm × 9–35µm for spindle and 8–20µm × 12–20µm for triangular (Table 3.8). Comparatively, these neuronal somas were more or less of

similar sizes to those found in the ventromedial field but appeared smaller if judged against somas in the distinct clusters of lateral motor field and medial motor field.

3.3.6 Ventromedial Field

As suggested by its name, the ventromedial field is situated ventromedially at the ventral horn (Figure 3.30, Figure 3.31). Margin between ventrolateral field and ventromedial field was deemed ambiguous seeing that their neuronal soma distributions were both considerably low; 3.17 and 5.50 mean total of cells, respectively compared to those of other fields (Table 3.6, Figure 3.24). The variation patterns of cell bodies were comparable between ventrolateral field and ventromedial field, with spindle and triangular somas showing equivalence in low quantity while the rest were almost negligible. Those recorded also were of comparable dimensions that measured 8–17µm × 15–34µm for spindle-shaped cells located in this field and 10–17µm × 16–26µm for the triangular ones (Table 3.8).

3.3.7 Lateral Motor Field

Lateral motor field was found on the lateral side of the ventral horn (Figure 3.30). This field usually contained the largest neuronal somas in the spinal grey, showing more variable in shapes and sizes. They measured, in width and length, at 6–29µm × 16–82µm for spindle-shaped somas, 9–32µm × 12–64µm for triangular somas, 9–30µm × 10–64µm for polygonal shaped somas and 8–25µm × 15–56µm for tear-like somas (Table 3.8). The ventrolateral accumulation of large somas was most apparent in spinal section coming from the cervical and lumbar intumescences. These somas exhibited a distinct palisade-like arrangement (Figure 3.32, Figure 3.33) where neurons were aligned parallel to one another in diagonal direction although sometimes, they also appeared in big clusters with no specific pattern. Very often, scattered among the larger

neurons are small population of small cells. In the thoracic and sacral segmental sections, this field was, however, occupied by smaller sized cells in no particular arrangement.

3.3.6 Medial Motor Field

Medial motor field was positioned at the medial corner of the ventral horn, consisting of darkly stained large somas that were mostly concentrated in the thoracic and sacral spinal sections whilst groups of smaller ones occurred in the cervical and lumbar spinal levels (Figure 3.30, Figure 3.32, Figure 3.34). These somas were usually grouped in clusters; each in random orientation. Spindle-shaped cells were occasionally found lying parallel to the ventral border of this field. Similarly to lateral motor field, the medial motor field also contained cell bodies of diverse somatal shapes, but they had slightly smaller perikaryal dimensions (in width and length); 7–22µm × 15–49µm for spindle-shaped somas, 7–24µm × 12–29µm for triangular somas, 6–29µm × 11–39µm for polygonal shaped somas and 7–17µm × 12–37µm for tear-like somas (Table 3.8). Somas in the form of spindle occurred most frequently, followed by triangular and polygonal shapes. Found in smaller number were the tear-shaped cell bodies and those of other forms. Such distribution pattern was similar in both lateral motor field and medial motor field, though they differed in the absolute number of recorded cells (Table 3.5, Figure 3.24)

.

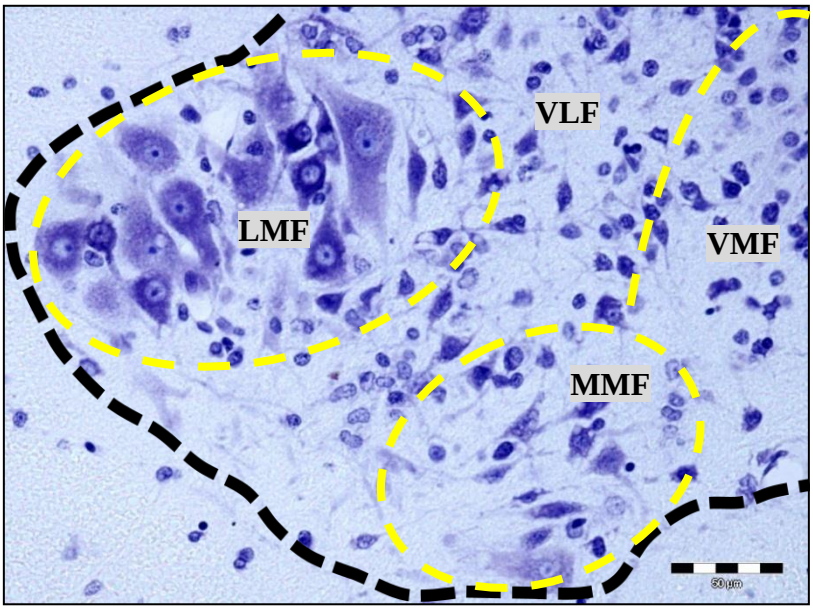

Figure 3.30: Field division of the ventral horn (Nissl, 200× magnification). [LMF: lateral motor field, MMF: medial motor field, VLF: ventrolateral field, VMF: ventrolateral field]

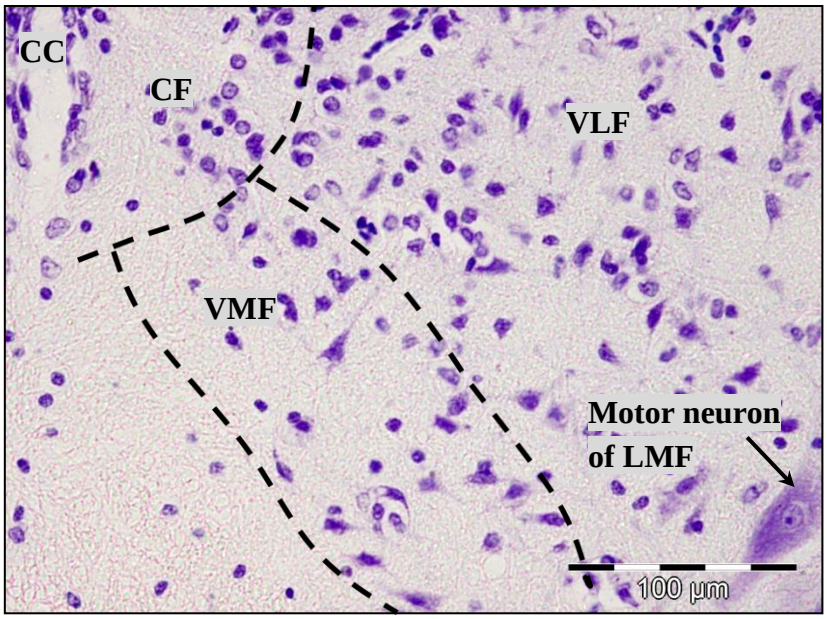

Figure 3.31: Ventrolateral field and ventromedial field (Nissl, 200× magnification). [CC: central canal, CF: central field, VLF: ventrolateral field, VMF: ventrolateral field]

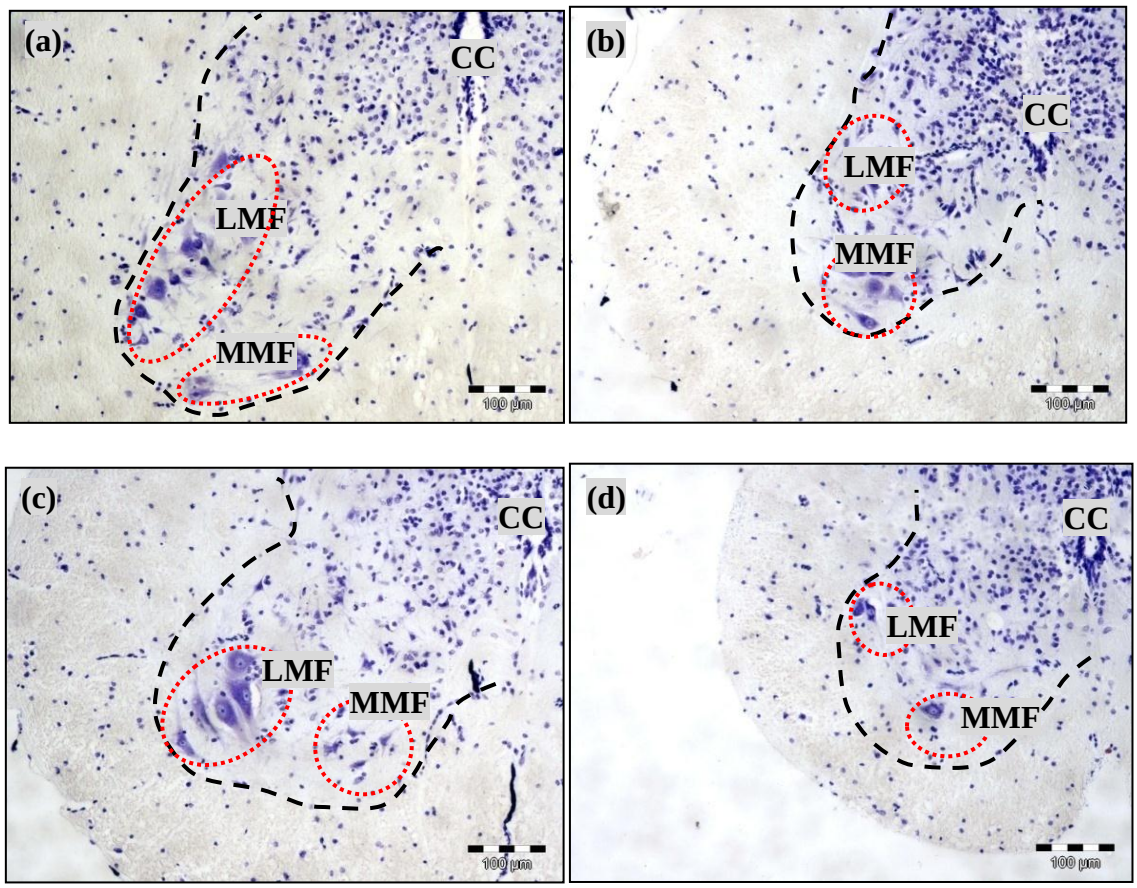

Figure 3.32: Location of motor neuron pool at different segmental levels; (a) cervical, (b) thoracic, (c) lumbar and (d) sacral (Nissl, 100× magnification). [CC: central canal, LMF: lateral motor field, MMF: medial motor field]

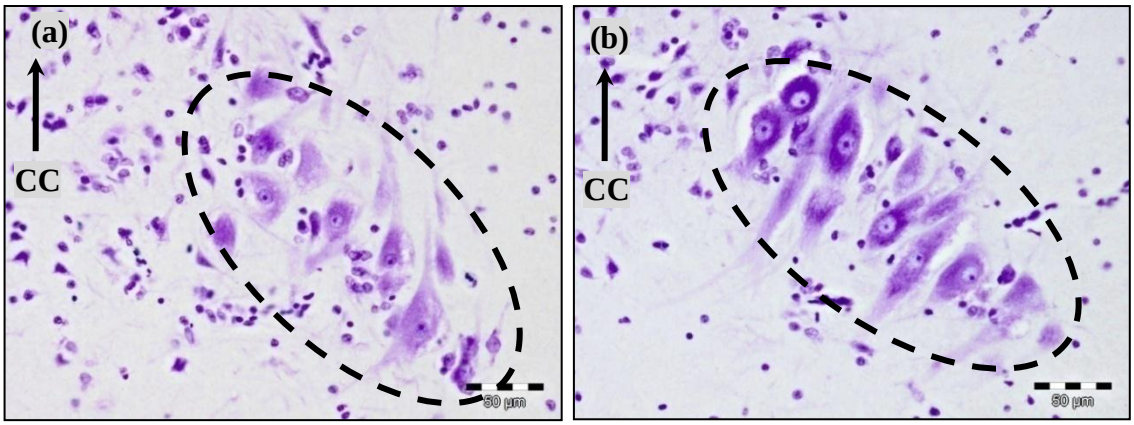

Figure 3.33: Palisade-like arrangement of motor neurons in lateral motor field of the (a) cervical and (b) lumbar spinal sections (Nissl, 200× magnification). [CC: central canal]

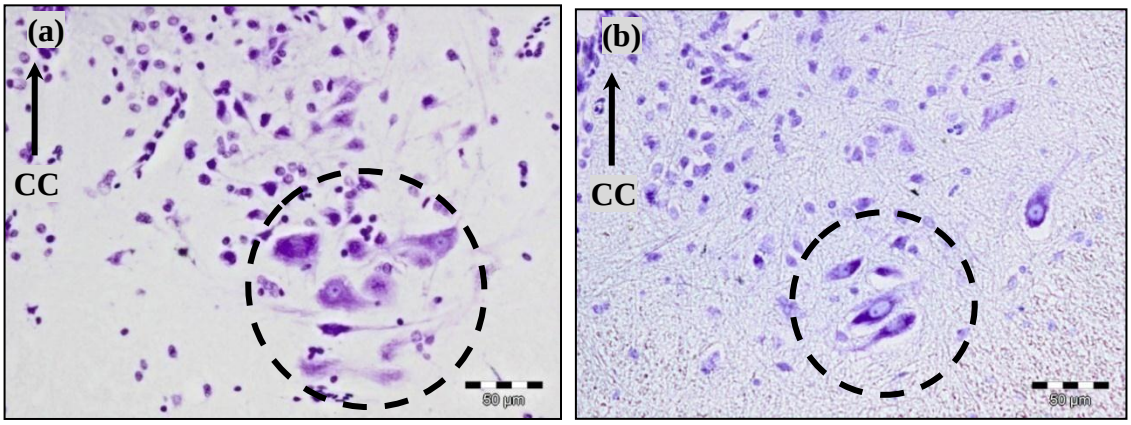

Figure 3.34: Motor neurons grouped in clusters in medial motor field of the (a) thoracic and (b) sacral spinal sections (Nissl, 200× magnification). [CC: central canal]

Table 3.8: Morphological profiles (in shape and range of size) of neuronal somas in different fields of spinal cord.

Field	Somatal shape	Somatal size in width × length, *μm*
Dorsal	Spindle Triangular	4–15 × 12–44 8–19 × 8–34
Lateral	Spindle Triangular Polygonal Tear	6–15 × 15–42 5–23 × 8–27 6–14 × 6–14 7–12 × 12–21
Central	Spindle	3–5 × 10–12
Ventrolateral	Spindle Triangular	8–20 × 9–35 8–20 × 12–20
Ventromedial	Spindle Triangular	8–17 × 14–34 10–17 × 16–26
Lateral motor	Spindle Triangular Polygonal Tear	6–29 × 16–82 9–32 × 12–64 9–30 × 10–64 8–25 × 15–56
Medial motor	Spindle Triangular Polygonal Tear	7–22 × 15–49 7–24 × 12–29 6–29 × 11–39 7–17 × 12–37

3.4 Localisation of Selected Nociception-related Neurotransmitters

The immunohistochemical localisation of the investigated nociception-related neurotransmitters, i.e. enkephalin (ENK), substance P (SP) and serotonin (5HT), were performed on the frog spinal cord representative sections for each segmental level. In the HRP-DAB immunostained spinal cord transverse sections at the light microscopic level, the positive immunoreactions for these neurotransmitters appeared as distinct dark brown particles. They were clearly distinguishable from the much lighter brown background staining for non-counterstained sections. Hematoxylin-counterstained sections on the other hand, provided a better contrast between the brown DAB reaction products and the blue background of the spinal cord sections, especially the foamy appearance of the white matter (Figure 3.35). In most cases, these dark brown reaction products were revealed in the form of varicose fibres that appeared as 'beads-on-string' structures and also individual bouton- or dot-like structures without intervaricose connections (Figure 3.36). These forms were interpreted to be the nerve fibres and their terminals in the respective order. The labeled fibres displayed both horizontal and vertical orientations. Some of the labeled elements were also seen in a cluster with seemingly a hollow centre. A profile as such was inferred as immunoreactive neuronal cell bodies with negatively stained nuclei for the particular tested neurotransmitter. Each batch of results was validated via control tests. Positive control slides were conducted with a known tissue to contain the antigens under study, which in this case, kidney and liver tissues of the investigated animal. These slides showed positive reaction with all three antibodies tested (Figure 3.37). In contrary, negative immunoreactivity was observed after the omission of primary antibody from the staining procedure in negative control (Figure 3.38). Regardless, one could never entirely rule out the slightest possibility of antibody crossreactivity with an antigen that is structurally related, for instance, the precursor molecule and its fragments that might produce false-positive

results. And for that reason, the positively labeled immunoreative elements of the investigated neurotransmitters in this study were denoted as ENK-, SP- and 5HT-like immunoreactivity (or in short, ENK-LI, SP-LI and 5HT-LI respectively).

Through microscopic observation, the intensity of the immunoreactions is scored according to the scale of 'high', 'moderate' and 'low' (Figure 3.35). ENK showed the highest staining intensity of fibre clusters followed by SP and finally 5HT (Figure 3.39). The distribution of ENK and SP in general, demonstrated an overlapping pattern as to having coinciding immunoreactive sites in spite of their labeled density. 5HT immunoreactivity on the other hand, slightly varied as it was found in the areas where positive ENK and SP immunoreactions were sparsely observed. By and large, ENK-, SP- and 5HT-like immunoreactivities were stronger in the upper part of the spinal cord section, i.e. dorsal and lateral fields, as compared to the ventral side. The distribution of the ENK-, SP- and 5HT-LI in the frog spinal cord transverse sections is summarised in Figure 3.39 and Table 3.9.

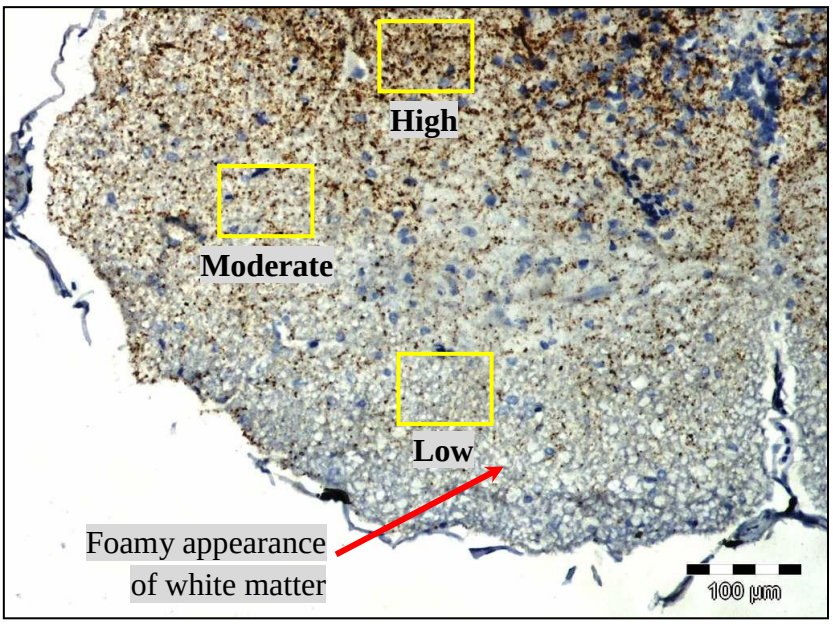

Figure 3.35: The scale of dark brown immunoreactivity concentration differentiated into 'high', 'moderate' and low'on an ENK-immunostained spinal cord section, counterstained in Hematoxylin (100× magnification). Also showing is the foamy appearance of the white matter.

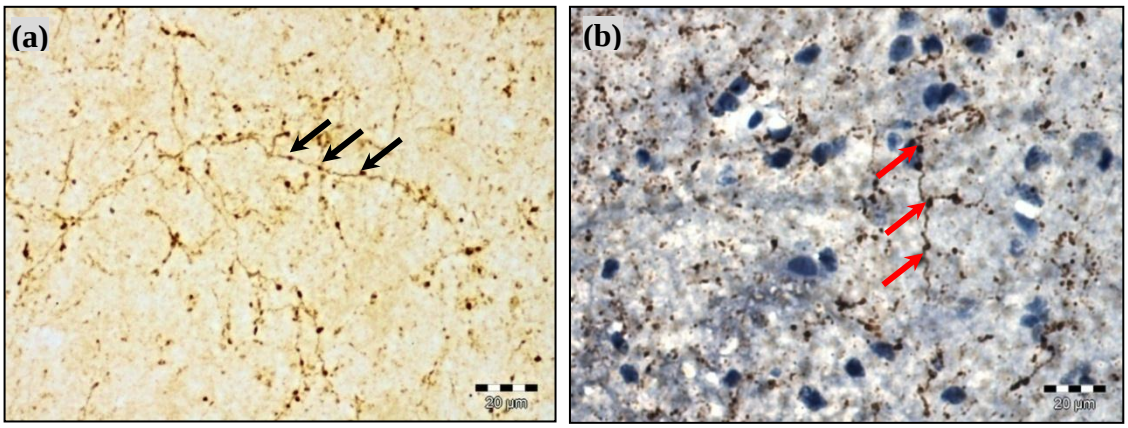

Figure 3.36: Immunoreactive fibres that appeared as distinct dark brown particles, in the form of beads-on-string structures, of a (a) non-counterstained section and (b) Hematoxylin counterstained section (400× magnification). As indicated by the arrows are the varicosities or terminals bonded by fibres.

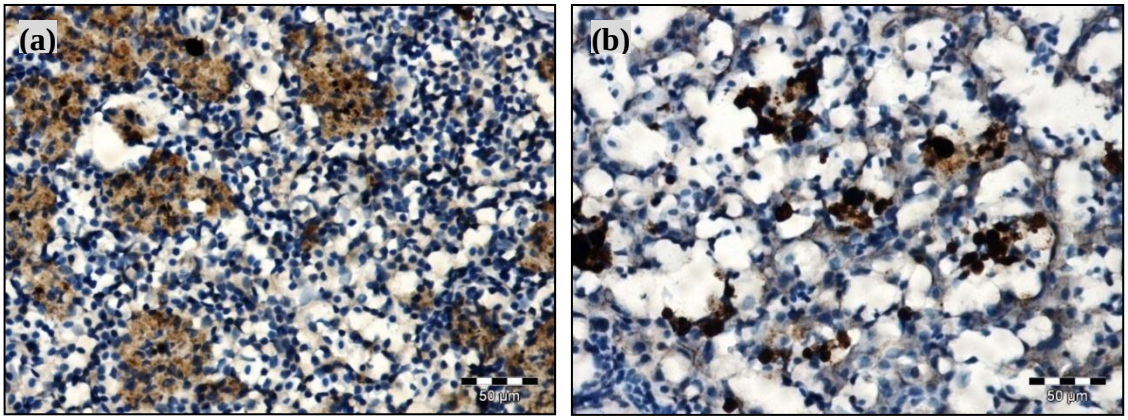

Figure 3.37: Positive control slides using (a) kidney tissue and (b) liver tissue of the experimental animal. Both revealed specific brown SP-like immunostaining (200× magnification).

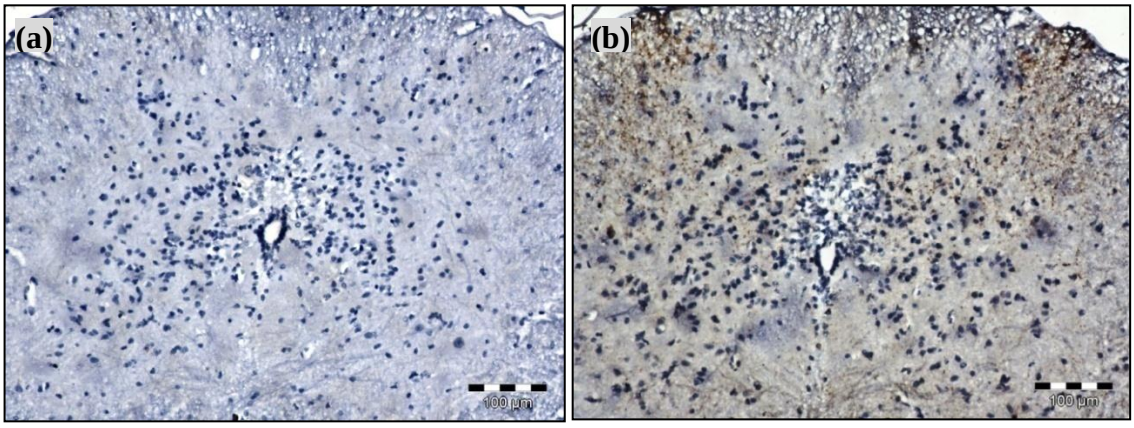

Figure 3.38: (a) A counterstained negative control section showing no brown-coloured reaction products, versus (b) immunostained section reacted with SP antibody (100× magnification).

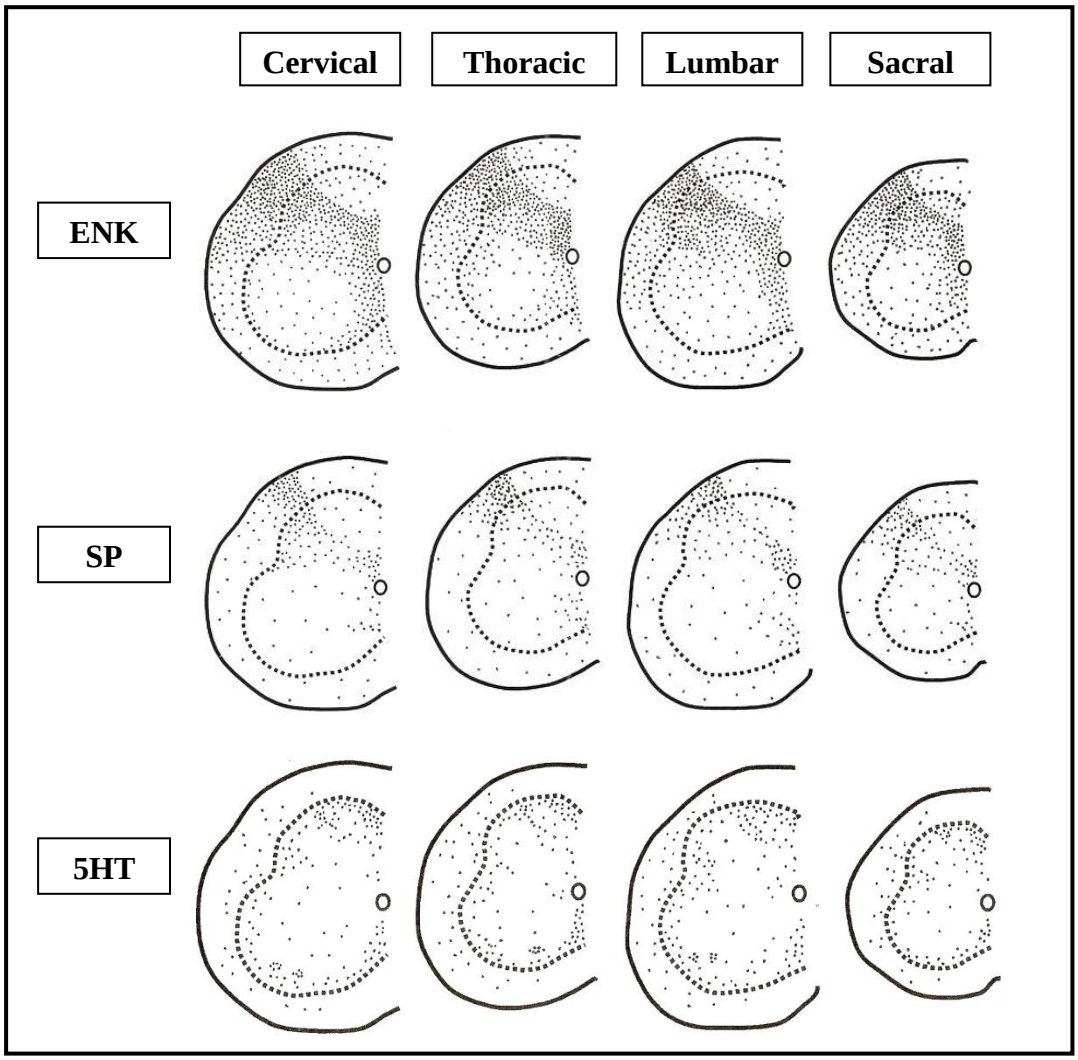

Figure 3.39: A schematic drawing showing comparative distribution of enkephalin- (ENK), substance P- (SP) and serotonin- (5HT) like immunoreactivities in transverse sections of the frog spinal cord.

Table 3.9: Distribution of enkephalin- (ENK), substance P- (SP) and serotonin- (5HT) like immunoreactivities in transverse sections of the frog spinal cord. Refer to Figure 3.35 for the scale of immunoreactivity concentration.

Presence of Immunoreactivity	ENK-LI	SP-LI	5HT-LI
1) Cell bodies	Present	Absent	Absent
2) Motor neurons	Absent	Absent	Present
3) Mediolateral band	Present	Present	Absent
4) Dorsal grey commissure	High	Moderate	Low
5) Ventral grey commissure	Moderate	Low	Moderate

3.4.1 Enkephalin-like Immunoreactivity

ENK-like imunoreactivity (ENK-LI) was generally found in all areas of the spinal cord transverse section including both grey matter and white matter (Figure 3.39, Figure 3.40). Notably detectable was a wide, dense band of dot- and fibre-like labeled structures that were confined to the ventral base of the dorsal funiculus or presumably the Lissauer's tract of the white matter. The Lissauer's tract covered the superficial area at the tip of the dorsal horn where primary afferent fibers that enter the dorsal root terminate in this area. The ENK-labeled band spread medially towards the lower portion of dorsal field, encompassing the whole area of the lateral field and anterior portion of the central field (dorsal grey commissure) (Figure 3.41). This cluster of fibres and varicosities was referred to as the mediolateral band. While this area exhibited the densest, the lowest ENK fibre density was demonstrated in the dorsal funiculus, dorsal field and the lateral motor field. The density of this positive elements band showed a decreasing vertical gradient in a dorsal to ventral direction. For the rest of the spinal cord section, ENK-LI fibres and varicosities were considered moderate. Such distribution pattern was consistently observed in all spinal cord segmental levels (Figure 3.40, Figure 3.41), though a much weaker version in terms of ENK-LI density was demonstrated in colchicine-treated animals (Figure 3.42). Both horizontally- and vertically-oriented ENK-LI fibres were also observed coursing throughout the spinal cord (Figure 3.43).

As for the localization of ENK-LI cell bodies in the grey matter, they were scattered in the medial region of the lateral field and sometimes appearing in the dorsal portion of central field. Commonly, they were found within the mediolateral band, in both normal and colchicine-treated animals. The latter demonstrated a higher number of labeled cells. These cell bodies occurred most frequently in the cervical and lumbar levels and

occasionally observed in the thoracic and sacral spinal segments. They largely appeared as ovoid-shaped with a single primary dendrite projection extending from one side of the cell body; in somatal size (in width and length) of 6–11µm × 8–22µm (Figure 3.44). A moderate number of the ENK-labelled cell bodies were spindle-shaped with two primary dendrites arising from the opposite poles; their dimensions ranging from 6.0–9.7µm × 13.6–23.3µm (Figure 3.44). A few were characterised as spherically shaped without any apparent extension from the cell body, which measured at 8–13µm wide and 9–15µm lengthwise (Figure 3.44). Most of them were seen directing towards the central canal while there were some rare cases in which the ovoid-shaped ENK-LI cell bodies were projected toward the opposite direction of the central field. Motor neurons in the lateral motor field and motor field did not reveal any form of positive immunoreactivity (Figure 3.45).

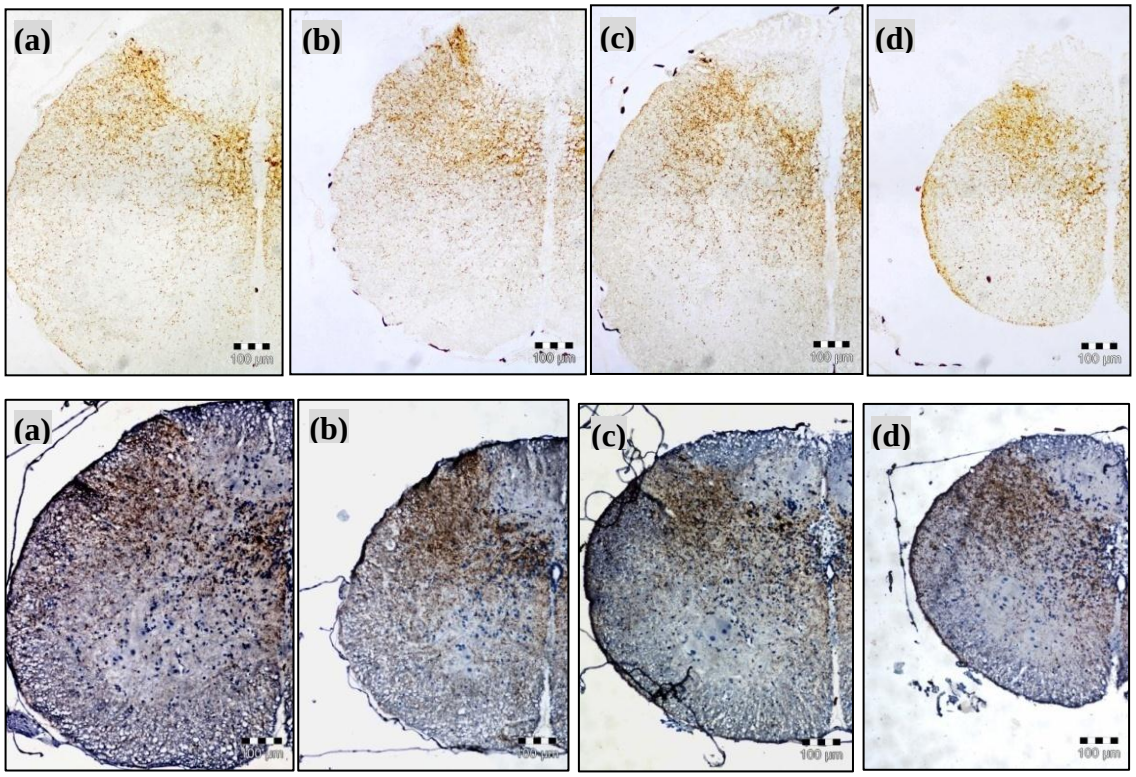

Figure 3.40: Distribution of ENK-like immunoreactivity at spinal cord segmental levels in non-counterstained sections (top row) and Hematoxylin counterstained sections (bottom row); (a) cervical, (b) thoracic, (c) lumbar and (d) sacral; (100× magnification).

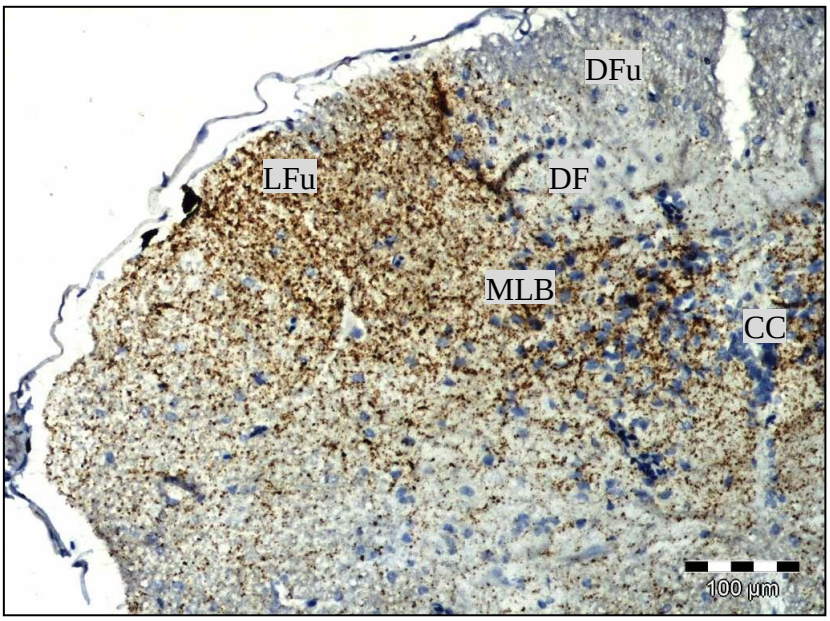

Figure 3.41: Distribution of ENK-like immunoreactivity in Hematoxylin counterstained frog spinal cord; (a) non-colchicine treated animal and (b) colchicine-treated animal (100× magnification). [CC:central canal, DF: dorsal field, DFu: dorsal funiculus, LFu: lateral funiculus, MLB: mediolateral band]

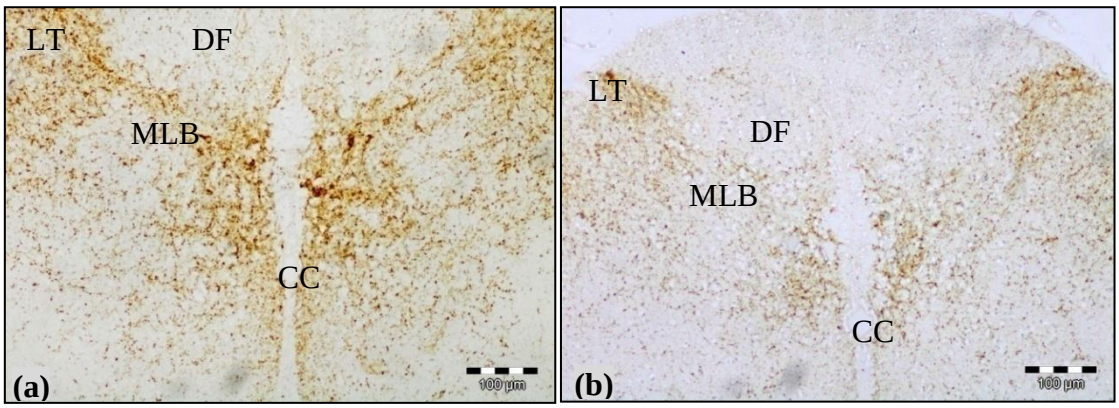

Figure 3.42: ENK-like immunoreactivity in frog spinal cord; (a) non-colchicine treated animal and (b) colchicines-treated animal, at cervical spinal segment (100× magnification). [CC:central canal, DF: dorsal field, LT: Lissauer's tract, MLB: mediolateral band]

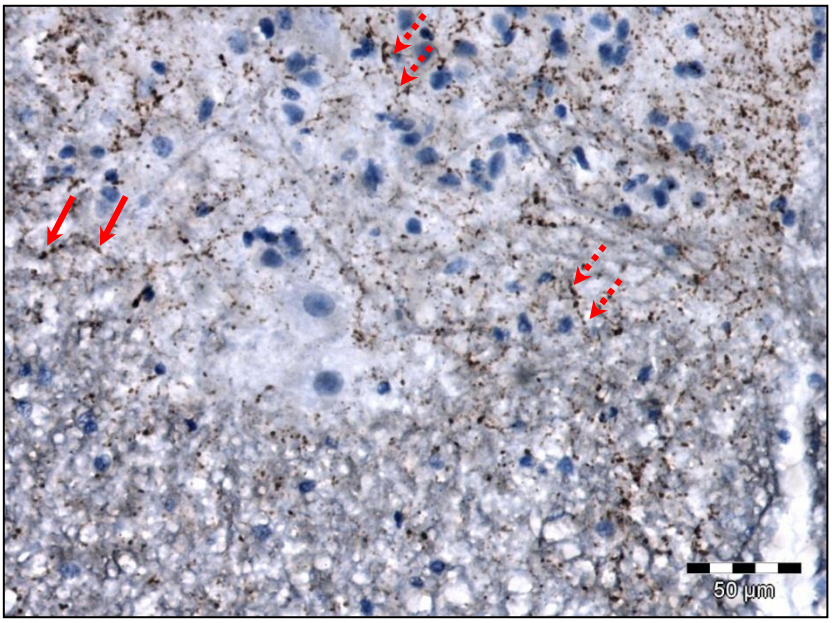

Figure 3.43: Horizontally (red arrow) and vertically (dotted-line red arrow) oriented ENK-labeled fibres (200× magnification).

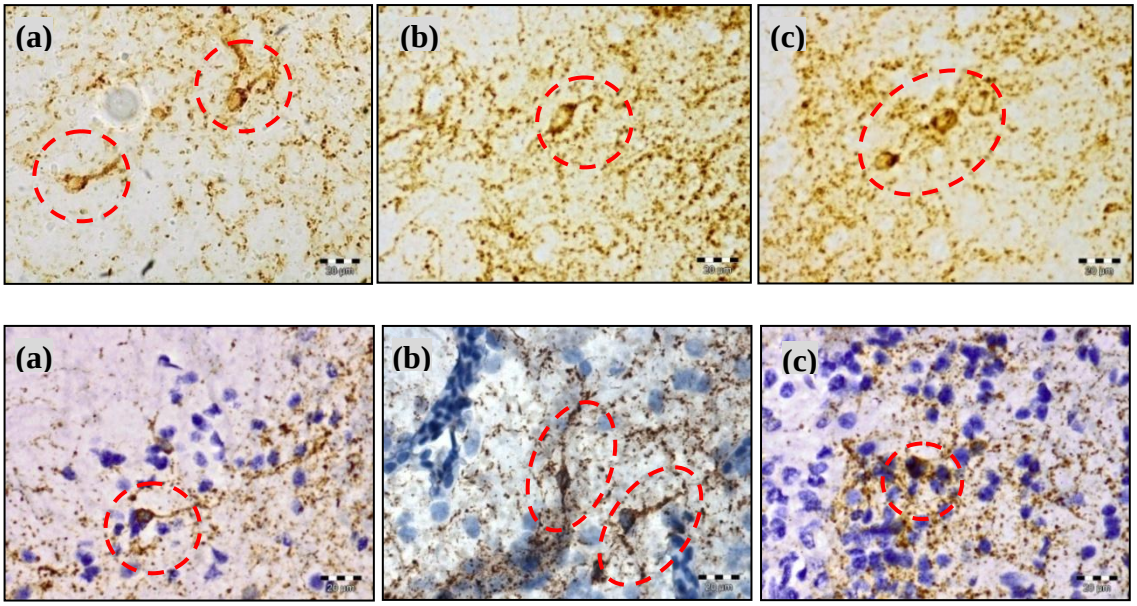

Figure 3.44: Various forms of ENK-like immunoreactive cell bodies (as indicated by the dotted circles) in the spinal cord at 400× magnification; (a) ovoid-shaped cell bodies with a single primary dendrite projection, (b) spindle-shaped with two primary dendrites arising from the opposite poles and (c) spherically-shaped cell bodies without any extension, in non-counterstained (top row) and Hematoxylin counterstained sections (bottow row).

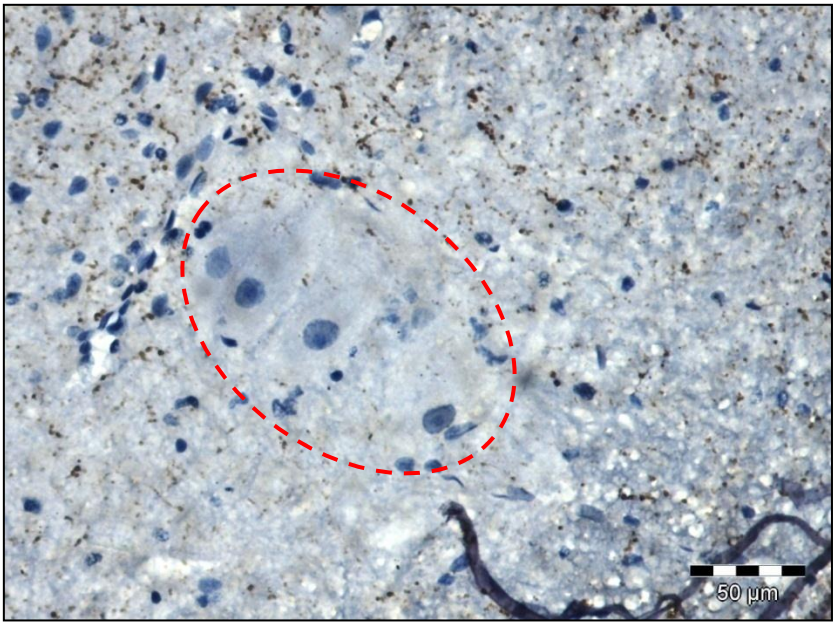

Figure 3.45: Absence of ENK positive immunoreactions within motor neuron area (dotted circle); (200× magnification).

3.4.2 Substance P-like Immunoreactivity

The positive reaction products of the substance P-like immunoreactivity (SP-LI) were present in all regions of the spinal cord cross sections for the four investigated segmental levels (Figure 3.39, Figure 3.46). SP-LI occurred in short fragments of varicose fibres and also individual varicosities or terminals, with the latter being more commonly found especially in the regions with lower immunoreactivty density (Figure 3.47). A prominent immunoreactivity band was revealed in similar areas where densest ENK-labeled particles were present. This horizontally oriented band was seen coursing medially from the ventral edges of dorsal funiculus and the upper region of lateral funiculus (presumably the Lissauer's tract). It extended to the base of the dorsal field, lateral field and upper areas of central field (dorsal grey commissure) or collectively regarded as the mediolateral band (Figure 3.48, Figure 3.49). Nonetheless, the intensity of SP-LI fibres and terminals were relatively less in comparison to those of ENK. At lower magnification, they were not readily observable due to the scattered distribution of SP-labeled sites (Figure 3.46, Figure 3.48). Their distribution steadily reduced in the

dorsal-to-ventral manner, exhibiting the rarest of SP-LI fibres and terminals in the upper dorsal field as well as the dorsal funiculus. The rest of the spinal cord region, which included of the ventral field and its white matter counterpart, the ventral funiculus were also showing scant immunoreactive varicosities dispersion. No SP-LI particles resided on the motor neurons (Figure 3.50). Unlike in ENK-immunostained spinal sections, SP labeled cell bodies were not detected at all levels, even in colchicine-treated animals.

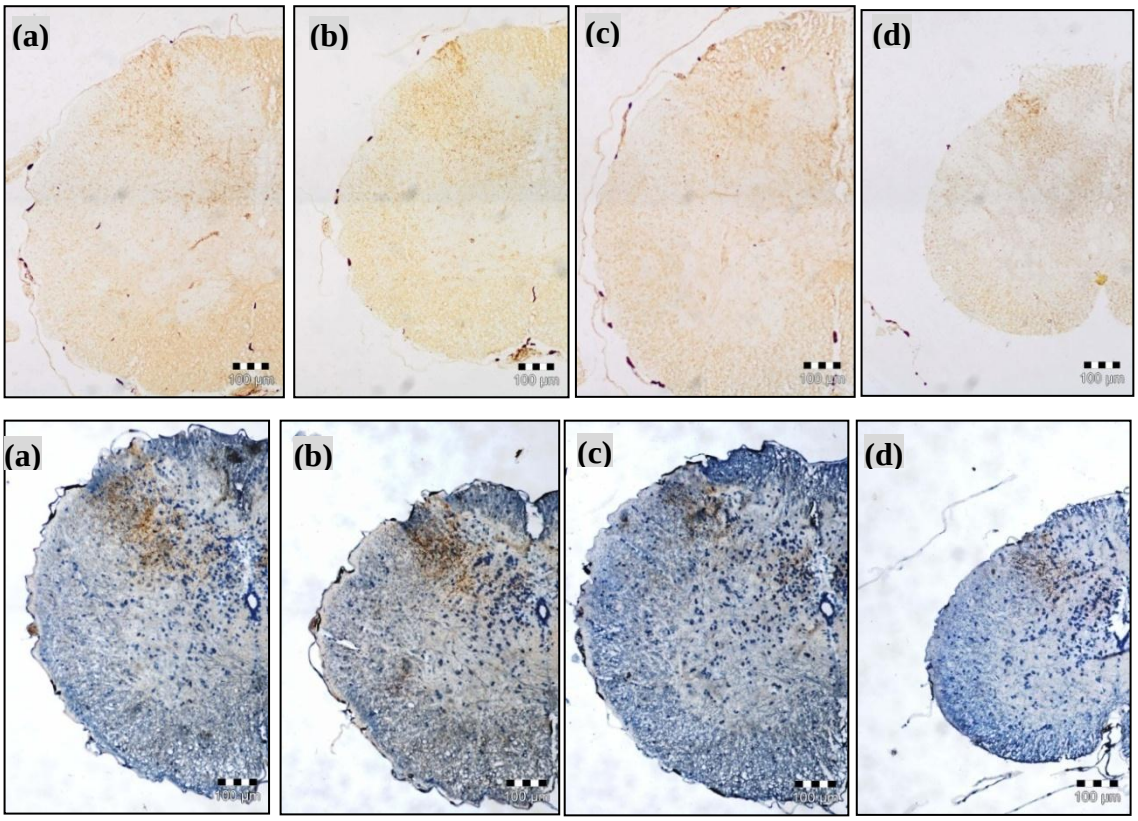

Figure 3.46: Distribution of SP-like immunoreactivity at spinal cord segmental levels in non-counterstained sections (top row) and Hematoxylin counterstained sections (bottom row) that was not readily observable at lower magnification; (a) cervical, (b) thoracic, (c) lumbar and (d) sacral; (100× magnification).

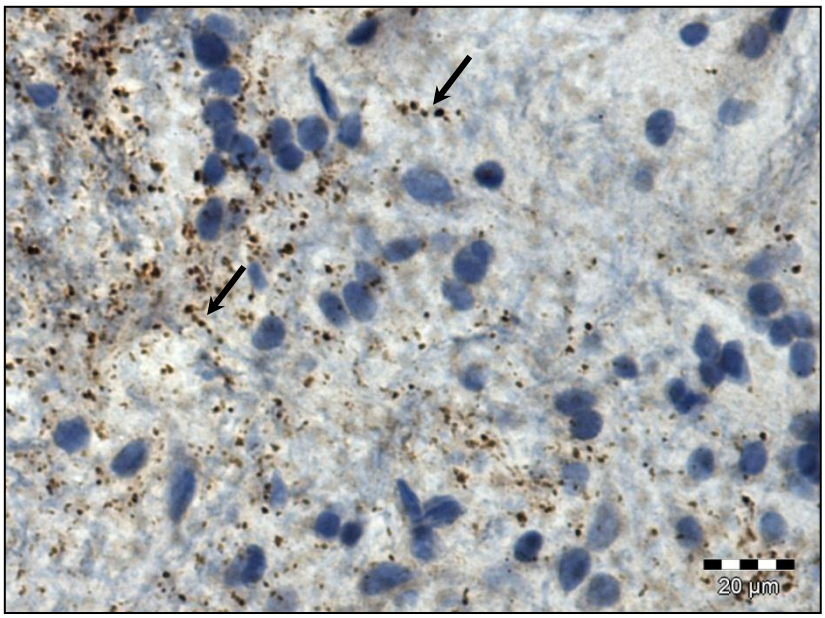

Figure 3.47: SP-like immunoreactivity occurred in short fragments of varicose fibres (indicated by arrows); (400× magnification).

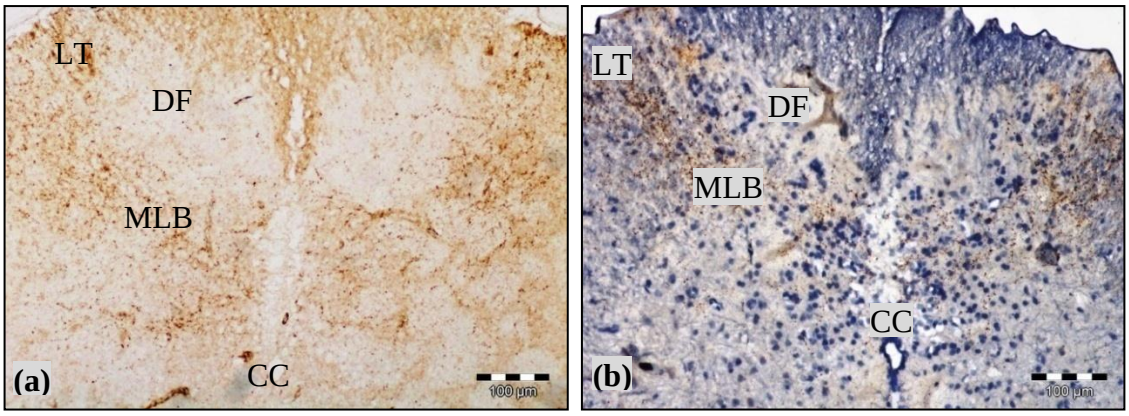

Figure 3.48: SP-like immunoreactivity in the frog spinal cord (100× magnification); (a) non-counterstained section and (b) Hematoxylin counterstained section. [CC:central canal, DF: dorsal field, LT: Lissauer's tract, MLB: mediolateral band]

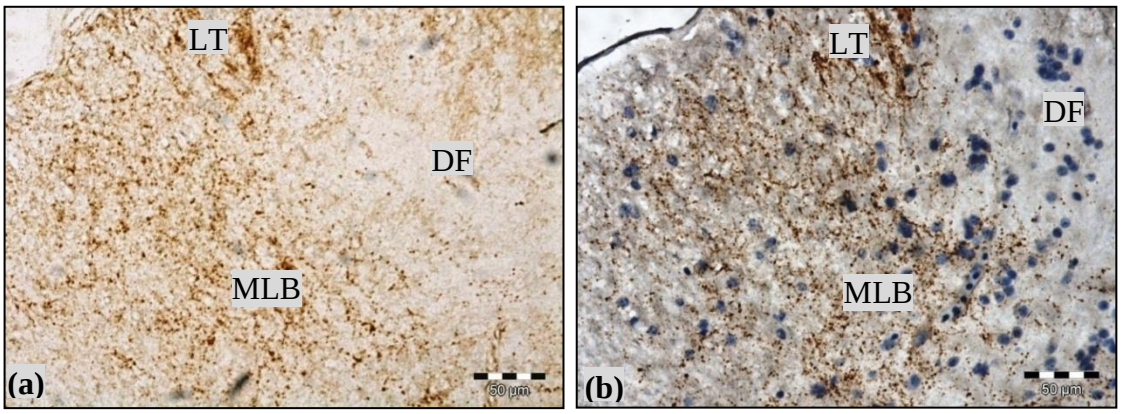

Figure 3.49: SP-like immunoreactivity at the Lissauer's tract (in-between region of dorsal and lateral funiculi), extending to the mediolateral band (200× magnification); (a) non-counterstained section and (b) Hematoxylin counterstained section. [DF: dorsal field, LT: Lissauer's tract, MLB: mediolateral band]

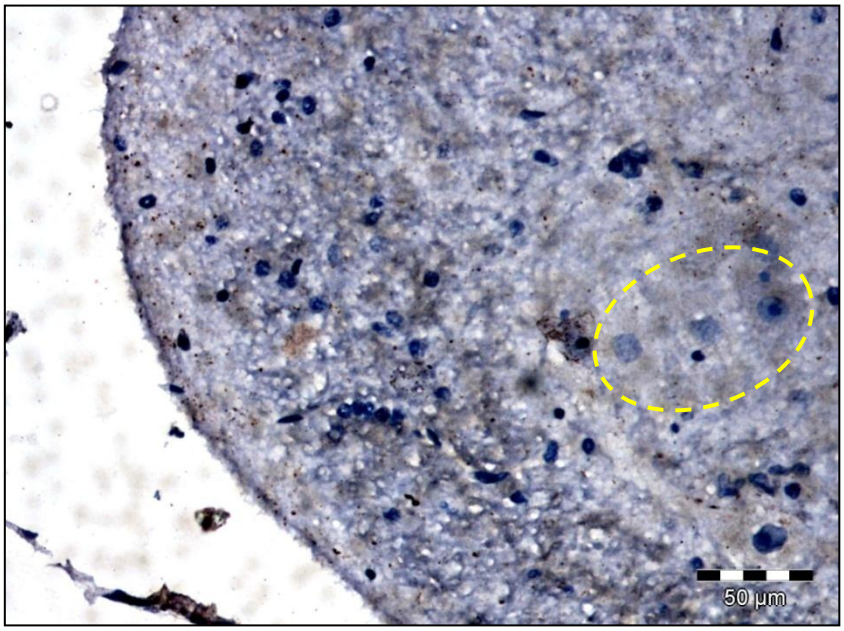

Figure 3.50: Absence of SP-like positive immunoreactions within motor neuron area (200× magnification).

3.4.3 Serotonin-like Immunoreactivity

The spinal cord showed a decreased concentration level of serotonin (5HT), revealing a much more dispersed distribution of positively-labeled fibres and varicosities or terminals compared to both ENK and SP (Figure 3.39). Likewise, these immunoreactive elements were not clearly noticeable under lower magnifications, which was attributable to the low expression of immunopositive sites (Figure 3.51). The 5HT-labeled individual varicosities were notably more frequent than those in the form of short varicose fibres.

5HT-like immunoreactivity (5HT-LI) was present throughout the grey and white matters with no definitive pattern. It was considerably more prominent in almost the entire region of dorsal field (Figure 3.52) compared to other areas, which contained moderately low amount of immunoreactive elements in an even distribution. 5HT labeled elements were seen present around the central field but primarily gathered in the ventral grey commissure (Figure 3.53) while ENK- and SP-LI were seen more commonly in the dorsal grey commissure (Figure 3.39). Most of the white matter areas had thinly scattered 5HT-LI labeling. There were immunoreactive varicosities around the margin between dorsal field and dorsal funiculus while the upper area of dorsal funiculus apparently showed almost no 5HT-LI of any form (Figure 3.54). In the ventral field, the motor neuron areas were occasionally found to exhibit 5HT-LI varicosities; though the motor neuron itself did not show any immunoreactions (Figure 3.55). This was in contrast to the absence of ENK- and SP-LI in these areas. However, no 5HT-labeled elements were found in any cell bodies, even in colchicine-treated animals, at all segmental levels.

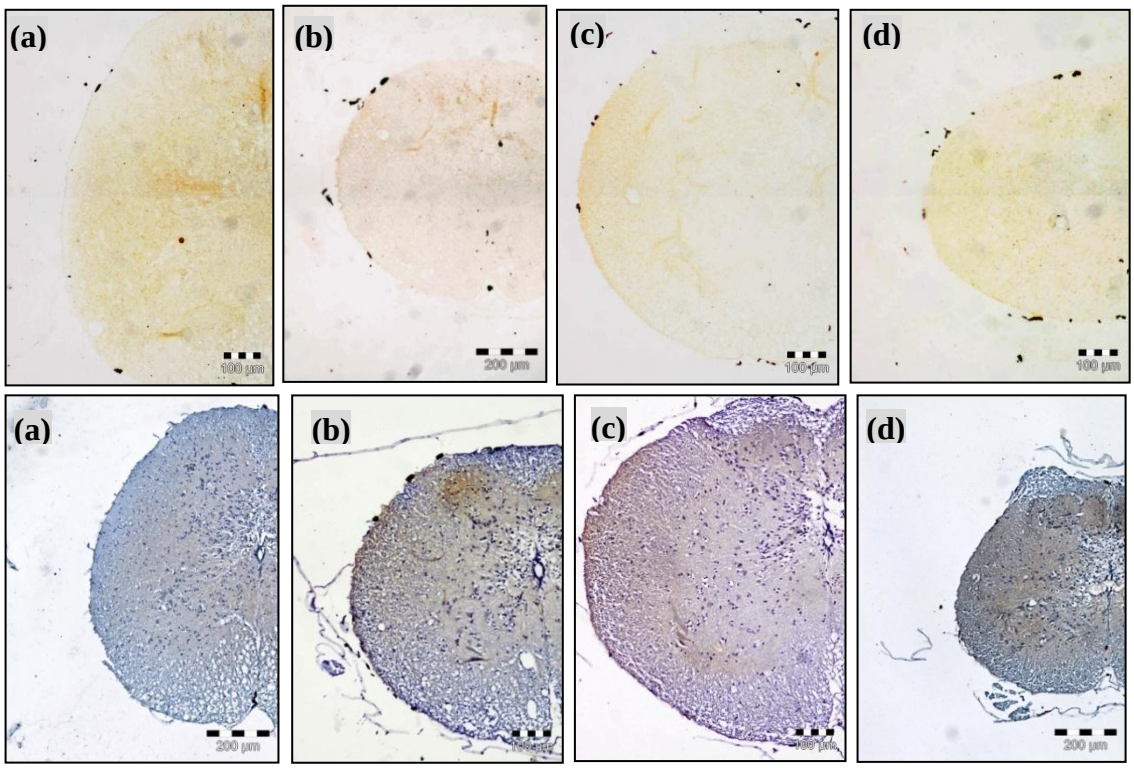

Figure 3.51: Distribution of 5HT-like immunoreactivity at spinal cord segmental levels in non-counterstained sections (top row) and Hematoxylin counterstained sections (bottom row) that was not readily observable at lower magnification; (a) cervical, (b) thoracic, (c) lumbar and (d) sacral; (100× magnification).

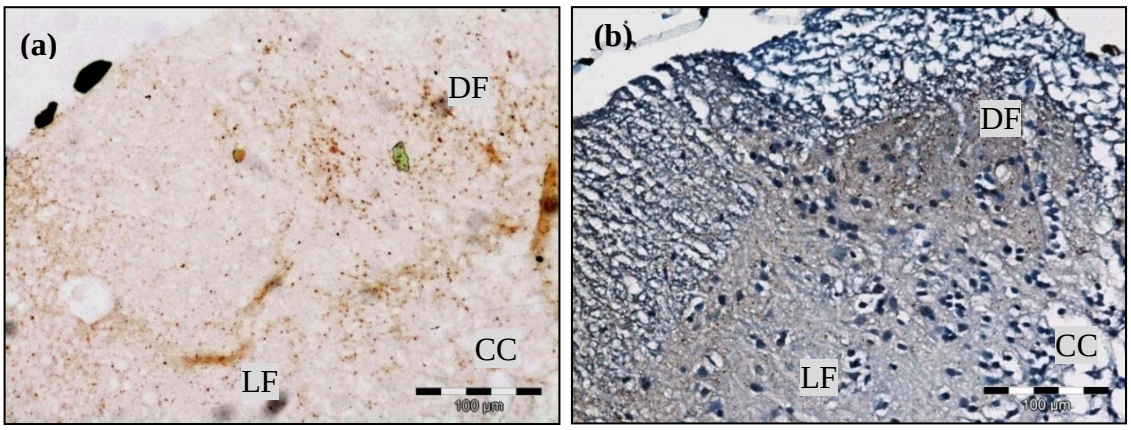

Figure 3.52: 5HT-like immunoreactivity at the dorsal field and lateral field (100× magnification); (a) non-counterstained section and (b) Hematoxylin counterstained section. [CC:central canal, DF: dorsal field, LF: lateral field]

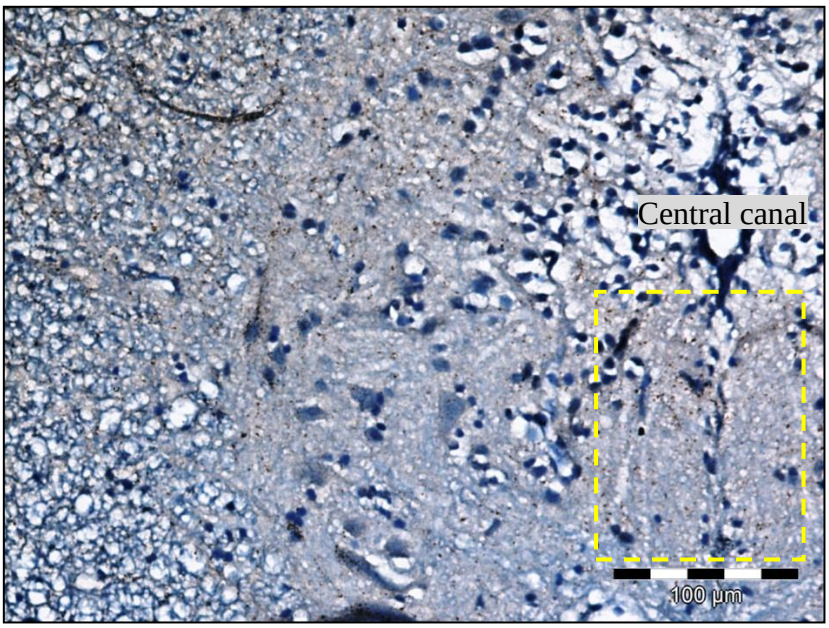

Figure 3.53: 5HT-like immunoreactive varicosities present in the ventral grey commissure (dotted line box); (100× magnification).

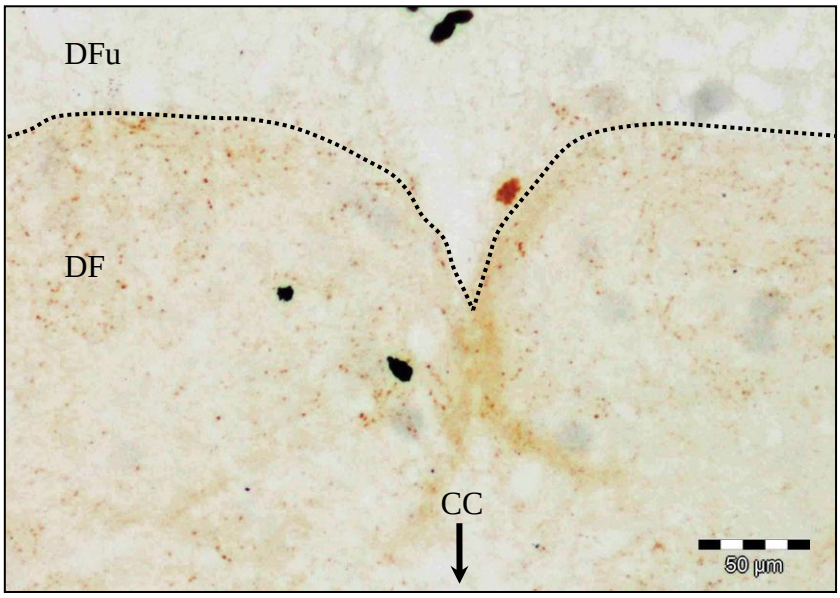

Figure 3.54: 5HT-like immunoreactivity in the dorsal field and dorsal funiculus (200× magnification). Dotted line depicts the presumable boundary between the grey matter and white matter. [DF: dorsal field; DFu: dorsal funiculus]

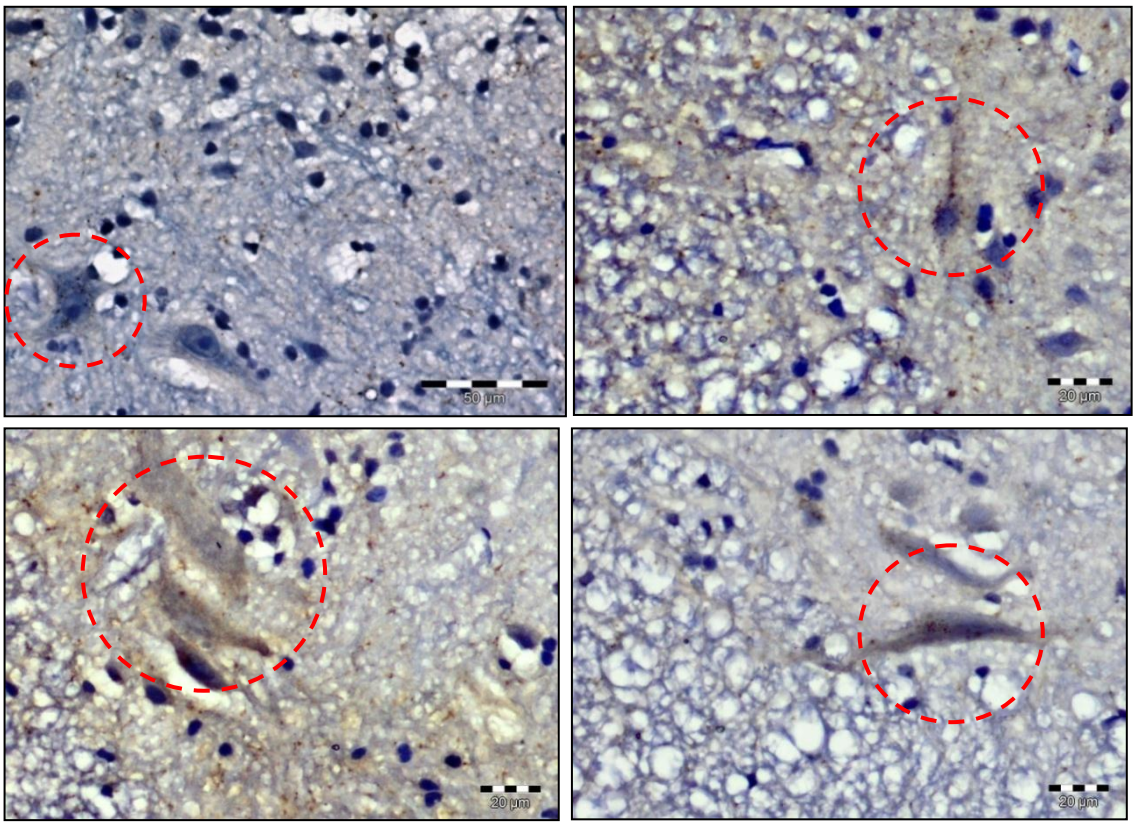

Figure 3.55: Visualisation of 5HT-like immunoreactive particles that resided in motor neurons (400× magnification).